BB

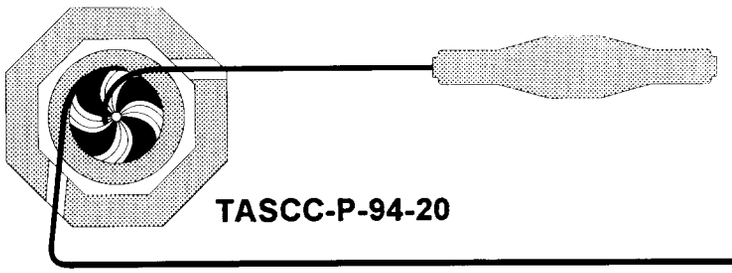

PREPRINT

tascc

TASCC-P-94-20

High Spin Proton and Neutron Intruder Configurations in ^{106}Cd.

P.H. Regan, A.E. Stuchbery, G.D. Dracoulis, A.P. Byrne[1], G.J. Lane, T. Kibédi
Department of Nuclear Physics, Research School of Physical Science and Engineering,
Australian National University, Canberra, ACT 0200, Australia

D.C. Radford, A. Galindo-Uribarri, V.P. Janzen, D. Ward
AECL Research, Chalk River Laboratories, Chalk River, Ontario, K0J 1J0, Canada

S.M. Mullins, G. Hackman
Department of Physics and Astronomy, McMaster University, Ontario, L8S 4M1, Canada

J.H. DeGraaf, M. Cromaz
Department of Physics, University of Toronto, Toronto, Ontario, M5S 1A7, Canada

S. Pilotte
Department of Physics, University of Ottawa, Ottawa, Ontario, K1N 6N5, Canada

[1]Joint appointment with The Department of Physics, The Faculties, The Australian National University, Canberra, ACT 0200, Australia

Submitted to Nucl. Phys. A

Physical and Environmental Sciences
Chalk River Laboratories
Chalk River, ON K0J 1J0 Canada

1994 September

High Spin Proton and Neutron Intruder Configurations in ^{106}Cd.

P.H. Regan, A.E. Stuchbery, G.D. Dracoulis, A.P. Byrne§, G.J. Lane, T. Kibédi

Department of Nuclear Physics, Research School of Physical Science and Engineering, Australian National University, Canberra, ACT 0200, Australia

D.C. Radford, A. Galindo-Uribarri, V.P. Janzen, D. Ward

AECL Research, Chalk River Laboratories, Chalk River, Ontario, K0J 1J0, Canada

S.M. Mullins, G. Hackman

Department of Physics and Astronomy, McMaster University, Ontario, L8S 4M1, Canada

J.H. DeGraaf, M. Cromaz

Department of Physics, University of Toronto, Toronto, Ontario, M5S 1A7, Canada

S. Pilotte

Department of Physics, University of Ottawa, Ottawa, Ontario, K1N 6N5, Canada

Abstract

High spin states in ^{106}Cd have been studied with the reactions ^{94}Zr(^{16}O,4n)^{106}Cd and ^{76}Ge(^{34}S,4n)^{106}Cd. A rotational band, based on a two-quasineutron $(h_{\frac{11}{2}})^2$ configuration, is observed from its 10^+ bandhead to spin 28 $\hbar$. This structure undergoes a band-crossing at a rotational frequency of approximately 0.45 MeV/$\hbar$, interpreted as the alignment of a pair of $g_{\frac{7}{2}}$ neutrons. Time-correlated spectroscopy has been used to identify states above the previously observed 12^+ isomer at 4660 keV. These include a weakly populated, strongly-coupled structure which indirectly feeds the isomer, and whose alignment and in-band decay properties are consistent with a deformed

$\nu(h_{\frac{11}{2}})^2\pi(g_{\frac{9}{2}}g_{\frac{7}{2}})$, four-quasiparticle configuration. The results are discussed in terms of cranked shell model and total Routhian surface calculations. No evidence is found for a reported 16^+ isomer at 7119 keV.

Key words: NUCLEAR REACTIONS ^{94}Zr(^{16}O,4n)^{106}Cd, E=88,92 MeV; ^{76}Ge(^{34}S,4n)^{106}Cd E=140 MeV; measured $\gamma-\gamma(t)$, E_γ, I_γ, DCO ratios, ^{106}Cd deduced levels J, π, B(M1)/B(E2) ratios, $\frac{|g_K-g_R|}{Q_0}$. Enriched targets, pulsed–beam, Ge hyper–pure, Compton suppressed detectors. Quasiparticle configurations, quasiparticle alignments, Cranked Shell Model calculations, Total Routhian Surface calculations.

Submitted to Nuclear Physics **A**

1st September 1994

§Joint appointment with The Department of Physics, The Faculties, The Australian National University, Canberra, ACT 0200, Australia.

I. INTRODUCTION.

Due to their proximity to the Z=50 closed shell, cadmium isotopes near A$\sim$105 are almost spherical at low spins and their excited states are well described as vibrational excitations [1]. However, the prolate deformation-driving nature of the neutron 'intruder' $[550]\frac{1}{2}^-$ orbital, from the $h_{\frac{11}{2}}$ subshell, can give rise to weakly deformed band structures at medium to high spins. Level schemes of odd-N isotopes $^{105-111}$Cd [2–5] are dominated at high spins by structures arising from the occupation of one or more of these orbitals. In the even-even isotopes, the recent studies of ^{108}Cd by Thorslund *et al.* [6,7] and of ^{110}Cd by Piiparinen *et al.* [8] and Juutinen *et al.* [9,10] have identified decoupled bands built upon 10^+ bandheads. The relatively long lifetimes of these 10^+ states (800 ps in ^{110}Cd and 51 ps in ^{108}Cd) led to their interpretation as intrinsic states arising from the deformed $\nu(h_{\frac{11}{2}})^2$ configuration. The heavier, even-N, cadmium isotopes exhibit deformed structures [1] which have been interpreted as 2-particle-4-hole proton excitations across the Z=50 shell gap. For deformations of $\beta_2 \sim 0.2$, the K=$\frac{1}{2}$ component of the $g_{\frac{7}{2}}$ proton orbital ($[431]\frac{1}{2}^+$) crosses the high-K $g_{\frac{9}{2}}$ orbitals, giving rise to deformed 0^+ bandheads and associated rotational bands. In the present work we have studied states in $^{106}_{48}Cd_{58}$ with heavy-ion induced reactions, with the aim of populating deformed configurations at high spin. A parallel study of this nucleus has recently been reported by Jerrestam *et al.* [11].

II. EXPERIMENTAL PROCEDURE AND DATA ANALYSIS.

Data on ^{106}Cd were obtained from experiments at the Australian National University (ANU) 14UD pelletron accelerator and the Tandem Accelerator Super Conducting Cyclotron (TASCC) facility at the AECL research laboratories, Chalk River, Canada.

A. ^{16}O+^{94}Zr Reaction.

The initial experiment was performed at the ANU with the reaction ^{94}Zr(^{16}O,4n)^{106}Cd at a beam energy of 92 MeV. The continuous beam was incident on a thin (550 μg/cm^2) enriched ^{94}Zr target. Emitted γ rays were detected with the array CAESAR [12], which has six detectors placed in pairs at angles of 48°, 97° and 145° relative to the beam direction. Each germanium-detector energy signal was accompanied by its own time signal, thereby allowing time differences between pairs of γ rays to be measured. A planar detector was incorporated into the array to increase the detection efficiency for low-energy γ rays. Approximately 80×10^6 $\gamma-\gamma$ coincidence events were recorded, of which 20% were associated with ^{106}Cd. The other main decay products were ^{105}Cd (5n), ^{102,103}Pd (α4n, α3n) and ^{104,105,106}Ag (p5n, p4n, p3n). A 4k by 4k prompt-$\gamma-\gamma$ coincidence matrix was constructed from these data with the condition that the time difference between pairs of γ rays be less than 15 ns.

To study transitions associated with decays from isomeric states, a second experiment was performed with a 4 mg/cm^2 natural Pb stopper pressed onto the back of the target to stop the residual nuclei. The beam was pulsed into bursts of $\sim$1 ns separated by 1.7 μs intervals. The beam energy for this second experiment was reduced from 92 to 88 MeV to increase the relative yield of ^{106}Cd. Each γ-ray signal was accompanied by its associated time signal measured with respect to a beam-related pulse train. An 'out-of-beam' prompt-$\gamma-\gamma$ matrix was constructed with the conditions that the individual γ rays occurred at least 40 ns after the beam pulse, and that each pair of γ rays occurred within 15 ns of each other. In order to identify states above isomers, an' early-delayed' matrix was constructed with the condition that the early γ ray was detected within 15 ns of the beam pulse and the delayed γ ray occurred between 30 and 850 ns after the beam pulse. To deduce lifetimes of isomeric states, the data were also sorted into a $\gamma-\gamma-$time cube. By taking background-subtracted γ-ray coincidence spectra gated on transitions below and above the isomers, time difference spectra between pairs of γ rays could be obtained.

B. $^{34}S+^{76}Ge$ Reaction.

The experiment performed at Chalk River utilised the reaction $^{76}Ge(^{34}S,4n)^{106}Cd$ at a beam energy of 140 MeV. The continuous beam was incident on two stacked thin (~750 $\mu g/cm^2$) enriched ^{76}Ge foils. The reaction brought in considerably more angular momentum than the $^{16}O+^{94}Zr$ combination (l_{max} ~58 $\hbar$ compared with ~45 $\hbar$) and it was hoped to extend the level scheme to higher spins. Emitted γ rays were detected with the Chalk River 8π γ-ray spectrometer [13] consisting of twenty Compton-suppressed germanium detectors placed in four rings of five detectors located at 37°, 79°, 101° and 143° with respect to the beam direction. The 70-element bismuth germanate (BGO) inner ball was used to measure the fold (K) and sum energy (H) associated with each event. An array of CsI(Tl) detectors [14], covering approximately 85 % of 4π steradians, was mounted inside the 8π spectrometer to detect light ions. The event trigger required a prompt coincidence involving a minimum of two Compton-suppressed germanium detectors and at least ten elements of the BGO-ball.

The data were first sorted into a matrix of γ-ray energy versus K and H. Projections were made on known transitions in $^{104,105,106}Cd$ and the associated H and K spectra were inspected. In order to optimise the proportion of ^{106}Cd in the matrix, a high-H cut was imposed on the data, along with the condition that no charged particles be detected. Of the 230 million prompt-$\gamma-\gamma$ events detected, approximately 50 million satisfied these conditions.

C. Spin Assignments.

Spin assignments were based on angular distribution and angular-correlation measurements. Some transition anisotropies relative to the beam direction were obtained from data taken during the 92 MeV $^{16}O+^{94}Zr$ experiment at the ANU. The A_2 values (assuming A_4=0) from these data are summarized in table I. Coincidence-gated angular-correlation (DCO) information was gained from both the ANU and Chalk River experiments. The analysis of the ANU data used the technique described by Byrne *et al.* [15] and Lane *et al.* [16].

A DCO ratio, R' can be given by

$$R' = \frac{I(\gamma_{1FB} \quad \text{gated by} \quad \gamma_{2FB}) + I(\gamma_{1FB} \quad \text{gated by} \quad \gamma_{2N})}{2I(\gamma_{1N} \quad \text{gated by} \quad \gamma_{2FB})} \tag{1}$$

where the subscript FB refers to either the 48° or 145° detectors and N refers to the 97° pair. For the geometry of the detectors in the CAESAR array, assuming a substate distribution, σ/J=0.25, stretched quadrupole-quadrupole coincidences give $R' \approx$1.45, whereas stretched pure quadrupole-dipole coincidences give $R' \approx$0.95. For mixed E2/M1, ΔJ=1 transitions, R' can vary between 0.45 and 1.80 depending on the sign and magnitude of the multipole mixing ratio, δ. For transitions which link states of the same spin ($J \rightarrow J$) 1.0$\leq R' \leq$1.6, again depending on the mixing ratio.

The Chalk River data were sorted into a matrix containing only coincidences between a 37° or 143° detector and a 79° or 101° detector. Background-subtracted spectra gated by known E2 transitions were projected onto both axes of the matrix and the ratio of counts in the peaks of interest in the two spectra, R'', was used as a measure of the multipolarity. R'' is defined by

$$R'' = \frac{I(\gamma_2(79°, 101°) \quad \text{gated by} \quad \gamma_1(37°, 143°))}{I(\gamma_2(37°, 143°) \quad \text{gated by} \quad \gamma_2(79°, 101°))} \tag{2}$$

where the 79°, 101° and 37°, 143° are the detector angles. For the geometry of the 8π spectrometer, if both transitions are stretched quadrupoles, R''=1.0. If γ_2 is a stretched dipole with a quadrupole admixture, R'' can lie between 0.25 and 1.25 depending on the mixing ratio and the degree of alignment. The value for a pure stretched dipole (ie. δ=0) is 0.56 for $\sigma/J = 0.25$. For a $J \rightarrow J$ transition, the calculated value is between 0.65 and 1.05. Therefore, while transitions with $R'' \leq$0.56 can be uniquely assigned as stretched dipoles, the ambiguity for states with $R'' \sim$1.0 cannot be resolved with the present data set, except by consideration of the decay pattern. The experimental DCO data for both the Chalk River and ANU experiments are summarized in figure 1 and table I.

III. EXPERIMENTAL RESULTS.

A partial level scheme for ^{106}Cd constructed in the present work is shown in figure 2. The transitions associated with ^{106}Cd together with their intensity and spin assignments are summarized in table I.

A. Level Scheme.

The out-of-beam $\gamma - \gamma$ data showed all the known transitions [17] that decay from the well-established 90 ns, four-quasiparticle isomer at 4660 keV [18,19]. A partial decay scheme showing the states fed by this isomer in the present work is given in figure 3. A spectrum gated by the 633 keV $2^+ \rightarrow 0^+$ transition in ^{106}Cd for the out-of-beam $\gamma - \gamma$ ^{16}O+^{94}Zr data is shown in the lower portion of figure 4. No new states below the isomer were identified in the present work but all the previously proposed decays were confirmed.

Early projections on transitions below the 4660 keV isomer were made and the resulting spectra summed to identify transitions above the isomer. This spectrum (the sum of the 224, 336, 552, 633, 646, 861, 875, 998, 1009 and 1069 keV gates) is shown in the upper portion of figure 4. The energies and relative intensities of the transitions identified above the 12^+ isomer are given in table II. Samuelson *et al.* [17] proposed the placement of a 593, 660 keV cascade on top of the 12^+ isomer, which we confirm. Other states above this isomer are reported for the first time.

The low-spin states of ^{106}Cd have been studied recently by Kampulainen *et al.* [1] with the (p,2nγ) reaction. Since heavy-ion induced reactions preferentially populate yrast or near-yrast states, many of the non-yrast states populated in the (p,2nγ) reaction are not observed in the present work. There are however a number of levels below 2.4 MeV which appear in both data sets, namely the 4^+ level at 2104.7 keV and the yrast states at 2330.5 keV (5^+), 1494.1 keV (4^+) and 632.8 keV (2^+). The new features of the decay scheme shown in figure 2 are the structure labelled band 1, the strongly-coupled structure labelled band 4,

and the non-collective excitations above the 12^+ isomer.

1. Band 1.

Band 1 is built on a 10^+ bandhead at 4816 keV. A prompt$-\gamma-\gamma$ coincidence spectrum that shows transitions in the band is displayed in figure 5. This structure decays through two branches, the 1028 keV transition into the new 8^+ level at 3788 keV and the 695 keV transition to the previously observed 9^+ state [17] at 4436 keV. The excitation energy of the 8^+ level at 3788 keV is fixed by decays to known states, such as the 1285, 1296 and 703 keV transitions to the 2504 (6^+), 2492 (6^+) and 3084 keV (7^-) states, respectively. Some of the γ rays associated with band 1 (602, 808 and 892 keV) and its decay out (1028 keV) have been assigned to ^{106}Cd by Klamra and Dafni [20], but their proposed placement is inconsistent with our data.

In their recent work on ^{106}Cd, Jerrestam *et al.* [11] also reported a decoupled band built on the 4816 keV 10^+ bandhead. There is however a discrepancy in the ordering of the transitions in this band between their scheme and ours. This has a large effect on the deduced alignment, and consequently on the interpretation of the structure of the band. Jerrestam *et al.* place the 602 keV transition as depopulating an isomeric 16^+ state at 7118 keV with a half-life of 11^{+6}_{-3} ns (τ=16^{+8}_{-4} ns) and with the 892 and 808 keV transitions in the subsequent cascade. We do not agree with their ordering and find no evidence for such an isomer. Instead we propose that the 602 keV γ ray depopulates a 12^+ state at 5419 keV, with the 808, 892 and 981 keV lines in cascade above and in that order. If the 808 and 892 keV transitions were placed below the 602 keV transition, as suggested by Jerrestam *et al.* the two lines should have approximately the same intensity in the 602 keV gate. Both our spectrum and that shown in figure 1 of reference [11], however, show a reduced intensity of the 892 keV line compared to the 808 keV line, consistent with our ordering.

Figure 6a shows the time-difference spectra between two prompt in-band transitions in the $\nu(h_{\frac{11}{2}})^2$ band in ^{106}Cd taken from the backed target ^{16}O+^{94}Zr reaction. Figure 6b shows

a time-difference spectrum gated by the proposed transitions above (981 keV) and below (602 keV) the isomeric 16^+ state reported by Jerrestam *et al.* Also shown is the calculated decay curve expected for an isomer with a mean-life of 11 ns (less than the reported lower limit). Our data show no evidence of an isomer. As a calibration for this analysis, we used the same method to measure the lifetime of the known $\frac{11}{2}^-$ isomeric bandhead [21] in ^{103}Pd, populated via the α3n channel in the same data set. By taking time projections of combinations of the 244 keV line which lies below the isomer with the first four transitions in the band built on the $\frac{11}{2}^-$ band [2], we obtained the decay curve shown in figure 6c. The reported half-life [21] for the $\frac{11}{2}^-$ state in ^{103}Pd is 25±2 ns (τ=36±3 ns), consistent with our measured value of τ=33±3 ns.

2. Bands 2 and 3.

Figures 7 and 8 show $\gamma - \gamma$ coincidence spectra illustrating bands 2 and 3. These bands, observed previously by Samuelson *et al.* [17] and Andrejtscheff *et al.* [19], are confirmed and extended.

3. Band 4.

Figure 9 shows a $\gamma - \gamma$ coincidence spectrum of a new structure, band 4. While the excitation energy of band 4 is not fixed, a minimum value for the (19^+) bandhead energy of 9319 keV can be established by the observed decay via the 1623 keV transition from the (20^+) state into the 8100 keV 18^+ level of band 1. About 50% of the strength of the band is observed to feed into the 18^+ state via this transition, but the lowest transition in the band (404 keV) does not appear to decay into the 18^+ state. As implied from the decay scheme in figure 2 and by the presence of members of band 4 in the spectrum shown in figure 4, some branching occurs to both the 12^+ isomer and to band 3. Unfortunately, since the decay out of the band is uncertain, the spin assignments are tentative.

IV. DISCUSSION.

Since the cadmium isotopes lie close to the Z=50 spherical shell gap, non-collective (spherical) as well as weakly deformed prolate structures are observed. The proton Fermi surface lies high in the $g_{\frac{9}{2}}$ shell and the breaking of a pair of these protons gives rise to the yrast 8^+ states. In ^{106}Cd, the long-lived ($\tau \approx 90$ ns) yrast, 12^+ state at 4660 keV [17–19] is formed by coupling the yrast 8^+ two-quasiproton state to a two-quasineutron $(d_{\frac{5}{2}})^2$ state. The measured g-factor [22,23] of 0.74(2) implies an almost pure $\pi(g_{\frac{9}{2}})^2\nu(d_{\frac{5}{2}})^2$ spherical configuration. The fact that no obvious band structure based on the 12^+ state has been observed in the present work is consistent with this interpretation.

Formation of deformed structures in the cadmium isotopes appears to require the occupation of one or more $h_{\frac{11}{2}}$ neutron orbitals, which are strongly down-sloping with increasing prolate deformation for N$\sim$58. The onset of deformation splits the degeneracy of the spherical subshell states and the Nilsson nomenclature is a more correct way of labelling the orbitals. Table III summarizes the Nilsson orbitals close to the proton and neutron Fermi surfaces for ^{106}Cd at small prolate deformations, together with their spherical parent and Cranked Shell Model (CSM) labels.

A. CSM and TRS Calculations.

The results of Total Routhian Surface [25] (TRS) and CSM calculations using a Woods-Saxon potential are shown in figures 10 and 11, respectively. The CSM calculations employed deformation parameters taken from the TRS calculations. The pairing strength was assumed to decrease with increasing rotational frequency as parametrised in reference [26], so that at ω=0.65 MeV/$\hbar$ the pairing strengths have fallen to half of their value at zero rotational frequency. These were taken to be Δ_π=1.20 MeV and Δ_ν=1.08 MeV, equivalent to 80 % of the "third-difference pairing", as defined in reference [27].

The experimental alignments for the bands in ^{106}Cd observed in the present work are

shown in figure 12. These were calculated using Harris reference parameters of $\mathcal{I}_0$=7.0 $\hbar^2$/MeV and $\mathcal{I}_1$=15.0 $\hbar^4$/MeV^3 together with K values of 0, 1, 1 and 5 for bands 1, 2, 3 and 4 respectively.

B. Analysis of Strongly-Coupled Bands.

1. $\frac{|g_K - g_R|}{Q_0}$ *Analysis.*

Deformation-aligned, or strongly-coupled bands, can be characterized by a quantity $\frac{g_K - g_R}{Q_0}$, where g_K and g_R are the g-factors of the intrinsic state and the collective core respectively and Q_0 is the intrinsic quadrupole moment.

In a rotational model, the multipole mixing ratio, δ, is given by,

$$\frac{\delta^2}{1+\delta^2} = \frac{2K^2(2I-1)}{(I+1)(I-1+K)(I-1-K)} \left(\frac{E_1}{E_2}\right)^5 \frac{I_\gamma(\Delta I=1)}{I_\gamma(\Delta I=2)} \tag{3}$$

where K is the angular momentum projection on the symmetry axis, I is the initial spin of the branching state, E_1 and E_2 are the dipole and quadrupole transition energies in MeV and I_γ is the relative γ-ray intensity. The magnitude of the quantity $\frac{|g_K - g_R|}{Q_0}$ is then given by,

$$\frac{g_K - g_R}{Q_0} = \frac{0.93 E_1}{\left(\sqrt{I^2-1}\right)\delta} \tag{4}$$

A given configuration corresponds with a specific g_K-value in a rotational model. For a multi-quasiparticle state, with $K = \sum_i \Omega_i$, the g-factor is given by,

$$K g_K = \sum_i \Omega_i g_\Omega \tag{5}$$

Therefore if g_R and Q_0 are assumed, the experimental values of $(g_K - g_R)/Q_0$ give an indication of the configuration.

2. Analysis With the Dönau Formalism.

If a band has both deformation-aligned and rotation-aligned components in its configuration, the above analysis is incorrect, nevertheless theoretical $B(M1)$ strengths can be estimated with the Dönau geometric formula [28].
For bands with no signature splitting,

$$B(M1) = \frac{3}{8\pi}\frac{K^2}{I^2}\{(g^{(1)} - g_R)(\sqrt{I^2 - K^2} - i_x^{(1)}) - (g^{(2)} - g_R)i_x^{(2)}\}^2 \tag{6}$$

where the superscripts (1) and (2) refer to the deformation-aligned and rotation-aligned configurations respectively.
The B(E2) values are given by,

$$B(E2 : I \rightarrow I-2) = \frac{5}{16\pi}{Q_0}^2\left(\frac{3(I-K)(I-K-1)(I+K)(I+K+1)}{(2I-2)(2I-1)I(2I+1)}\right) \tag{7}$$

where I is the initial spin and K is the angular momentum projection on the axis of symmetry. The experimentally derived B(M1)/B(E2) ratios can then be compared with the predicted values for assumed quasiparticle configurations.

Experimental B(M1)/B(E2) ratios, in units of $(\frac{\mu_N}{eb})^2$ are given by,

$$\frac{B(M1)}{B(E2)} = 0.697\left(\frac{E_2^5}{E_1^3}\right)\frac{1}{1+\delta^2}\frac{I_\gamma(\Delta I = 1)}{I_\gamma(\Delta I = 2)} \tag{8}$$

C. Band 1: $\nu(h_{\frac{11}{2}})^2$ Structure.

The TRS calculations for the lowest positive-parity, even-signature configuration for ^{106}Cd predict that at small rotational frequencies, non-collective prolate states (γ=–120°) are favoured. Particularly favoured is the yrast 8^+ state that arises from the maximally-aligned two-quasiproton $\pi(g_{\frac{9}{2}})^2$ configuration. However, as figure 10(b) shows, at ω=0.569 MeV/$\hbar$, (corresponding to angular momentum $I \approx$18 $\hbar$), the prolate $\nu(h_{\frac{11}{2}})^2$ configuration becomes yrast with a predicted deformation of β_2=0.16. The two-quasineutron $(h_{\frac{11}{2}})^2$ configuration (EF) is predicted by the CSM calculations (see fig 11) to become favoured over the vaccum configuration at frequencies close to ω=0.40 MeV/$\hbar$ for ^{106}Cd. As figure 12 shows, there is an increase in alignment of $\sim$10 $\hbar$ between the ground-state band and band 1 in ^{106}Cd, consistent with a $\nu(h_{\frac{11}{2}})^2$ assignment to band 1. Similar increases in alignment are observed in the yrast bands of ^{108}Cd and ^{110}Cd [6,9,10] and in the even-even palladium isotopes from $^{104-108}$Pd [29–31].

It is important to note that the 10^+ state at 4816 keV is observed to decay to the 8^+ state at 3788 keV, but not to the yrast 8^+ state at 3044 keV. A similar decay pattern [6,8] was observed for the analogous 10^+ level in ^{108}Cd and ^{110}Cd. In ^{108}Cd, the 10^+ state at 4154 keV decays [6,7] strongly to the 8^+ state at 3684 keV (E_γ=470 keV) but only very weakly to the yrast 8^+ two-quasiproton state at 3111 keV (E_γ=1043 keV). Similarly, in ^{110}Cd the transition strength of the decay from the 10^+ state at 3611 keV is approximately 150 times stronger to the 8^+ member of the ground state band at 3275 keV than to the yrast, two-quasiproton 8^+ state at 3187 keV. Furthermore, the lifetimes for the 10^+ states in ^{108}Cd and ^{110}Cd of 51 and 800 ps respectively [7,8], imply that they are intrinsic states, whereas lifetimes of the band members above the 10^+ levels in ^{108}Cd and ^{110}Cd suggest deformations of $\beta_2 \approx$0.16 as predicted for the aligned $\nu(h_{\frac{11}{2}})^2$ configurations by the TRS calculations.

The upper panel of figure 13 displays the energy of the 10^+ level associated with the $\nu(h_{\frac{11}{2}})^2$ neutron configuration in the even-N cadmium isotopes as a function of mass number. It is clear that the excitation energy of this configuration rises for the lighter cadmium

isotopes. This is consistent with the observed energies of the yrast $\frac{11}{2}^-$ states in the odd-N isotopes, (associated with the population of the $[550]\frac{1}{2}^-$ one-quasineutron orbital) shown in the lower panel of figure 13, which also increases with decreasing neutron number.

The alignment plot for band 1 (see figure 12) shows a second increase of approximately 4 $\hbar$ at $\omega \sim$0.45 MeV/$\hbar$, close to the predicted frequency for the alignment of the $g_{\frac{7}{2}}$ neutron (AB) orbitals (see fig 11). Evidence for the alignment of these quasiparticles has recently been reported [2] in the one-quasiparticle $\nu h_{\frac{11}{2}}$ band for ^{105}Cd, as shown in figure 12.

The proposed ordering of the transitions in band 1 by Jerrestam *et al.* [11] led them to deduce a larger increase in the alignment than in the present work, which they interpreted as a band crossing with the high-K, $\nu(h_{\frac{11}{2}})^2\pi(g_{\frac{9}{2}})^2$ structure. Such a structure [6] has been reported in ^{108}Cd by Thorslund *et al.* but it displays a strongly-coupled character, with strong cascade ΔI=1 transitions and B(M1)/B(E2) ratios $\geq$100 $(\frac{\mu_N}{eb})^2$. Since band 1 appears to be decoupled up to spin 28^+, a similar configuration is not consistent with our experimental data.

D. Bands 2 and 3: Negative Parity Configurations.

Samuelson *et al.* [17] interpreted bands 2 and 3 in terms of a particle-rotor model to be bands built on 8^- and 9^- bandheads formed from the fully-aligned $\nu(h_{\frac{11}{2}}d_{\frac{5}{2}})$ and $\nu(h_{\frac{11}{2}}g_{\frac{7}{2}})$ configurations, respectively. However, due to the large B(E2) of the 188 keV transition between the 8^- state in band 2 and the 6^- state at 3319 keV, Kostov *et al.* [32] interpreted band 2 as a semi-decoupled structure, which starts from the 6^- level. To explain the non-observation of odd-spin members of the proposed semi-decoupled $\nu(h_{\frac{11}{2}}d_{\frac{5}{2}})$ structure, and even-spin members of the proposed rotation-aligned $\nu(h_{\frac{11}{2}}g_{\frac{7}{2}})$ bands, Kostov suggested that they would be populated less intensely than the competing yrast configurations. Non-yrast 9^- and 11^- states at 4114 and 4903 keV associated with the $\nu(h_{\frac{11}{2}}d_{\frac{5}{2}})$ band were reported by Samuelson *et al.*, but were not observed in the present work.

Since band 3 contains one-quasiparticle components from both the $h_{\frac{11}{2}}$ and $g_{\frac{7}{2}}$ neutron

orbitals, both of the first two predicted neutron alignments should be blocked. The alignment for band 3 is shown in figure 12. There are no large increases in alignment, which is consistent with the proposed configuration. There is however, a small increase of approximately 2 $\hbar$ between ω=0.5 and 0.6 MeV/$\hbar$. The CSM calculations for β_2=0.16 predict that the first $g_{\frac{9}{2}}$ proton (ab) alignment should occur close to this frequency, with a gain in alignment of approximately 2$\hbar$.

E. Band 4: The Strongly-Coupled Band.

While the decay path from band 4 is not precisely defined, the spin and parity of the bandhead are restricted and tentatively assigned as 19^+. The large initial alignment of this band (i_x $\sim$16 $\hbar$), as shown in figure 12, together with its strong decay into band 1, imply a rotation-aligned, prolate $\nu(h_{\frac{11}{2}})^2$ component in its configuration. (There are no competetive oblate configurations which would result in such a large initial alignment. For oblate deformations, the low-Ω, $g_{\frac{9}{2}}$ proton orbitals which reside close to the Fermi surface for Z$\approx$48 can generate a maximum of 8$\hbar$ of aligned angular momentum, however, the corresponding neutron Fermi surface for ^{106}Cd lies in the mid-Ω region of the $g_{\frac{7}{2}}$ shell and these orbitals can not contribute enough additional alignment to be consistent with band 4.)

The possible deformation-aligned components which could couple to the prolate deformed, $\nu(h_{\frac{11}{2}})^2$ rotation-aligned component are summarized in table IV. In terms of their spherical parent labels, these are: (1) $\pi(g_{\frac{9}{2}})^2\nu(g_{\frac{7}{2}}d_{\frac{5}{2}})$; (2) $\pi(g_{\frac{9}{2}})^2$; (3) $\nu(g_{\frac{7}{2}}d_{\frac{5}{2}})$; and (4) $\pi(g_{\frac{9}{2}}g_{\frac{7}{2}})$.

Figure 14 shows the expected B(M1)/B(E2) ratios for the four suggested configurations together with the experimentally derived values. It is clear that the two configurations that include two $g_{\frac{9}{2}}$ protons predict much larger values than those observed experimentally. The large theoretical values are due to a combination of the large g-factor for the $g_{\frac{9}{2}}$ proton (+1.27) and the large K-value associated with breaking a pair of these orbitals. (This

expectation is confirmed in ^{108}Cd, where Thorslund *et al.* [6] observe a strongly-coupled band with B(M1)/B(E2) ratios greater than 100 $(\frac{\mu_N}{eb})^2$, consistent with the $\nu(h_{\frac{11}{2}})^2\pi(g_{\frac{9}{2}})^2$ configuration, where one unpaired proton occupies the $[413]\frac{7}{2}^+$ Nilsson orbit and the other occupies the $[404]\frac{9}{2}^+$ orbit.)

In contrast, the predicted branching ratios for the $(h_{\frac{11}{2}})^2(g_{\frac{7}{2}}d_{\frac{5}{2}})$, four-quasineutron configuration are considerably lower than those observed experimentally. In our analysis we have assumed g-factor values consistent with pure $g_{\frac{7}{2}}$ and $d_{\frac{5}{2}}$ neutron orbitals for this configuration. However, these orbitals are heavily mixed at $\beta_2 \sim 0.15$ and the calculated g-factors for the mixed $[411]\frac{3}{2}^+$ and $[413]\frac{5}{2}^+$ orbitals in the Nilsson model tend to cancel out, resulting in a g-factor for the deformation-aligned part of equation 6 of close to zero. This has the effect of reducing the predicted B(M1)/B(E2) value even more when compared with the experimental values. In addition, the four-quasineutron configuration does not provide enough initial alignment to be consistent with that observed for band 4.

Both the calculated branching ratios (assuming a quadrupole moment of $Q_0 \sim 2.4$ eb, appropriate for $\beta_2 \sim 0.2$), and the expected initial alignment for the $\nu(h_{\frac{11}{2}})^2\pi(g_{\frac{9}{2}}g_{\frac{7}{2}})$ configuration are consistent with the experimental values. The formation of this configuration requires some explanation, however. The $[431]\frac{1}{2}^+$ proton orbital from the $g_{\frac{7}{2}}$ spherical subshell lies close to the Fermi surface for the cadmium isotopes for deformations of $\beta_2 \sim 0.2$, where it crosses the Z=50 shell gap and gives rise to prolate deformed configurations. Deformed 0^+ states with a two-particle-four-hole $\pi(g_{\frac{7}{2}})^2(g_{\frac{9}{2}})^{-4}$ configuration are well-known features of the heavier cadmium isotopes [1], and a decoupled band associated with a one-quasiproton $g_{\frac{7}{2}}$ configuration has also been recently observed in the Z=49 nucleus, ^{109}In [33].

For K=5 and Q_0=2.4 eb, the experimental values for $|g_K - g_R|$ are given in table V. Assuming $g_R \sim 0.4$ for the collective g-factor, we can derive average values for g_K that are approximately either $+1.1\pm0.1$ or -0.3 ± 0.1. Assuming values of K and g_K of 1 and –0.21 for the $\nu(h_{\frac{11}{2}})^2$ rotation-aligned component, and 4 and 1.20 for the

$\pi([413]\frac{7}{2}^+ \otimes [431]\frac{1}{2}^+)$ deformation-aligned component, respectively, the predicted value of g_K for the $\nu(h_{\frac{11}{2}})^2\pi(g_{\frac{9}{2}}g_{\frac{7}{2}})$ configuration is approximately +1.0, consistent with the positive experimental value.

F. Comparison with N=58 Isotones.

In order to understand the role played by the protons close to the Z=50 shell gap, it is appropriate to compare the decay schemes of the N=58 isotones, where differences in structure should be affected by proton excitations only. Up to medium spins, ^{106}Cd and ^{104}Pd have similar features. The ^{104}Pd decay scheme of Grau *et al.* [29] features a 10^+ bandhead at 4.023 MeV, similar to that observed here in ^{106}Cd. In addition, two negative-parity side-bands, analogous to bands 2 and 3 in the present work, were also observed, starting from 8^- and 9^- bandheads. The work of Macchiavelli *et al.* [30] extended the ground state band past the $\nu(h_{\frac{11}{2}})^2$ alignment to a tentative spin of 26^+. There is a second rise in the alignment in the ground state band of ^{104}Pd at about spin 20^+ and $\omega \sim 0.6$ MeV/$\hbar$, which may be due to the alignment of the $g_{\frac{7}{2}}$ neutrons, as observed in ^{106}Cd. In ^{104}Pd, an intense ($\sim$15% of the total ^{104}Pd yield) high-spin rotational structure has also been reported which may be based on a highly- or super-deformed shape [30]. No comparable structure was observed for ^{106}Cd in the present work. Similar bands have been reported in ^{103,105}Pd [30,34], though none have been reported in other N=58 isotones. This may suggest that it is the deformed proton shell-gap at Z=46 which is the crucial factor in the population of these structures.

While there are some similarities between ^{104}Pd and ^{106}Cd, the decay scheme of the semi-magic isotone ^{108}Sn is quite different [35]. Above the Z=50 shell gap, the structures are dominated by proton excitations from the $g_{\frac{7}{2}}$ and $h_{\frac{11}{2}}$ subshells, while below, the collective structures appear to be dominated by $h_{\frac{11}{2}}$ neutron excitations.

V. SUMMARY AND CONCLUSIONS.

In summary, we have studied high-spin states of the N=58 nucleus ^{106}Cd with (HI,xn) reactions. We observed a collective band structure built upon a 10^+ bandhead at 4816 keV which we associate with a two quasineutron, rotation-aligned $(h_{\frac{11}{2}})^2$ structure. The excitation energy of the deformed bandhead for this structure increases with decreasing neutron number through the known even-N cadmium isotopes. The decay of this band bypasses the yrast 8^+ two-quasi proton state, consistent with its decay pattern in the heavier isotopes. The rotation-aligned $(h_{\frac{11}{2}})^2$ band undergoes a perturbation at $\omega \sim 0.45$ MeV/$\hbar$ which is interpreted as a bandcrossing with the aligned four-quasineutron $(h_{\frac{11}{2}})^2 \otimes (g_{\frac{7}{2}})^2$ configuration, as suggested by cranked shell model and total Routhian surface calculations. A small rise in alignment in the previously observed two-quasineutron $h_{\frac{11}{2}} \otimes g_{\frac{7}{2}}$ band is possibly due to a proton alignment. No evidence is found of the previously reported 16^+ isomer at 7119 keV in this nucleus. A strongly-coupled band is reported at high spins in this nucleus for the first time. The large alignment and deduced $|g_K - g_R|$ values for this structure are consistent with a 4-quasiparticle band arising from the coupling of rotation-aligned $\nu(h_{\frac{11}{2}})^2$ and deformation-aligned $\pi(g_{\frac{7}{2}} g_{\frac{9}{2}})$ configurations.

Acknowledgements

Dr. R.M. Clark (Berkeley) is thanked for important discussions regarding the interpretation of the Total Routhian Surface and Cranked Shell Model calculations. Drs. S.S. Anderssen, P.M. Davidson, P.M. Walker, K.C. Yeung and the technical staff at the 14UD accelerator are thanked for their assistance during the ANU experiments. Mr. R. MacLeod is thanked for his help during the Chalk River experiment. Mr. R. Turkentine is thanked for preparing the enriched ^{94}Zr target. PHR and AES acknowledge the receipt of a grant from the Access to Major Facilities Overseas Program by the Australian Department of Industry, Science and Technology (DIST). Some of the data were analysed with the help of the analysis programs SLICE, GF2 and ESCL8R [36]. This work was in part supported by the Natural Sciences and Engineering Research Council of Canada, and AECL Research.

TABLES

TABLE I. Transitions observed in ^{106}Cd in the present work.

E_γ^a (keV)	I_γ	$E_i \rightarrow E_f$ (keV)	R'	R''	A_2	$J_i^\pi \rightarrow J_f^\pi$
171.1	3(2)	3678.1→3507.0	0.83(6)[b]	0.82(12)[f]	−0.13(15)	$9^- \rightarrow 8^-$
187.6	5(2)	3507.0→3319.4	1.25(11)[c]	0.99(15)[f]	+0.24(8)	$8^- \rightarrow 6^-$
223.6	—	4659.8→4436				$12^+ \rightarrow 10^+$
225.8	2(1)	2330.5→2104.7				$5^+ \rightarrow 4^+$
269.1	5(2)	3678.1→3409.0	1.15(13)[c]	1.09(12)[f]		$9^- \rightarrow 7^-$
311.6	2(1)	3678.1→3366.5		0.68(15)[f]	−0.13(8)	$9^- \rightarrow 8^+$
315.0	—	4436 →4120.9				$10^+ \rightarrow 9^+$
335.7	—	4659.8→4323.7				$12^+ \rightarrow 11^-$
403.6	4(2)	9722+x→9319+x				$(20^+ \rightarrow 19^+)$
422.8	6(2)	3507.0→3084.3	0.72(25)[j]	0.71(13)[j]		$8^- \rightarrow 7^+$

Table I cont.

E_γ^a (keV)	I_γ	$E_i \rightarrow E_f$ (keV)	R'	R''	A_2	$J_i^\pi \rightarrow J_f^\pi$
433.4	7(2)	3787.5→3353.8	0.99(18)[e]			$8^+ \rightarrow 7^+$
438.5	7(2)	10161+x→9722+x				$(21^+ \rightarrow 20^+)$
502.6	5(2)	10664+x→10161+x				$(22^+ \rightarrow 21^+)$
504.4	5(2)	11168+x→10664				$(23^+ \rightarrow 22^+)$
524.2	14(3)	2628.9→2104.7	0.79(8)[b]	0.70(10)[j]		$5^- \rightarrow 4^+$
540.9	13(3)	3044.2→2503.5	1.27(25)[g]	0.91(9)[d]		$8^+ \rightarrow 6^+$
552.8	20(3)	3044.2→2491.8	1.40(18)[f]	0.98(11)[f]		$8^+ \rightarrow 6^+$
571.0	4(2)	12311+x→11740+x			−0.58(17)	$(25^+ \rightarrow 24^+)$
572.5	4(2)	11740+x→11168+x				$(24^+ \rightarrow 23^+)$
592.5	6(2)	3084.3→2491.8	0.81(19)[f]			$7^- \rightarrow 6^+$
598.3	16(5)	4105.7→3507.0	1.23(19)[b]			$10^- \rightarrow 8^-$

Table I cont.

E_γ^a (keV)	I_γ	$E_i \rightarrow E_f$ (keV)	R'	R''	A_2	$J_i^\pi \rightarrow J_f^\pi$
602.4	40(7)	5418.8→4815.9	1.20(13)[d]	0.93(5)[d]		$12^+ \rightarrow 10^+$
610.6	15(5)	2104.7→1494.1	0.96(15)[b]	1.16(22)[j]		$4^+ \rightarrow 4^+$
632.8	130(10)	632.8→0.0	1.21(15)[d]	0.83(8)[d]		$2^+ \rightarrow 0^+$
633.9	14(6)	3678.1→3044.2				$9^- \rightarrow 8^+$
639.7	4(2)	12951+x→12311+x				$(26^+ \rightarrow 25^+)$
645.6	41(10)	4323.7→3678.1	1.59(22)[b]	0.93(9)[f]		$11^- \rightarrow 9^-$
663.3	4(2)	13614+x→12951				$(27^+ \rightarrow 26^+)$
690.5	14(4)	3319.4→2628.9	1.28(10)[b]	0.79(11)[j]		$6^- \rightarrow 5^-$
695.3	7(3)	4815.9→4120.9	0.66(20)[e]	0.50(9)[e]		$10^+ \rightarrow 9^+$
703.3	13(5)	3787.5→3084.3	0.72(20)[e]	0.50(9)[e]		$8^+ \rightarrow 7^+$
718.8	2(1)	14322+x→13614+x				$(28^+ \rightarrow 27^+)$

Table I cont.

E_γ^a (keV)	I_γ	$E_i \rightarrow E_f$ (keV)	R'	R''	A_2	$J_i^\pi \rightarrow J_f^\pi$
733.0	2(1)	15065+x→14322+x				$(29^+ \rightarrow 28^+)$
754.2	6(3)	3084.3→2330.5		1.02(20)[j]		$7^+ \rightarrow 5^+$
780.6	10(4)	3409.0→2628.9				$7^- \rightarrow 5^-$
795.6	2(1)	15861+x→15065+x				$(30^+ \rightarrow 29^+)$
807.9	42(11)	6226.7→5418.8	1.34(29)[g]	0.94(4)[d]		$14^+ \rightarrow 12^+$
827.4	5(2)	3319.4→2491.8	1.03(48)[b]			$6^- \rightarrow 6^+$
836.4	≤1	2330.5→1494.1				$5^- \rightarrow 4^+$
842.4	2(1)	10161+x→9319+x				$(21^+ \rightarrow 19^+)$
861.3	107(10)	1494.1→632.8	1.45(12)[d]	0.93(10)[d]		$4^+ \rightarrow 2^+$
861.3	18(7)	4967.0→4105.7				$12^- \rightarrow 10^-$
862.3	13(5)	3353.8→2491.8				$7^+ \rightarrow 6^+$

Table I cont.

E_γ^a (keV)	I_γ	$E_i \rightarrow E_f$ (keV)	R'	R''	A_2	$J_i^\pi \rightarrow J_f^\pi$
874.7	9(4)	3366.5→2491.8				$8^+ \rightarrow 6^+$
889.8	36(13)	5213.5→4323.7	1.20(31)[h]	0.95(5)[f]		$13^- \rightarrow 11^-$
892.3	38(13)	7119.0→6226.7	1.53(16)[d]	1.13(11)[d]		$16^+ \rightarrow 14^+$
906.0	6(3)	3409.0→2503.5		0.66(17)[f]		$7^- \rightarrow 6^+$
917.6	6(3)	3409.0→2491.8	0.75(18)[i]	0.69(13)[f]		$7^- \rightarrow 6^+$
941.5	5(2)	10664+x→9722+x				$(22^+ \rightarrow 20^+)$
980.8	32(11)	8099.8→7119.0	1.29(16)[e]	1.02(5)[d]		$18^+ \rightarrow 16^+$
997.7	51(12)	2491.8→1494.1	1.51(23)[h]	0.92(7)[e]		$6^+ \rightarrow 4^+$
1007.0	4(2)	11168+x→10161+x				$(23^+ \rightarrow 21^+)$
1008.6	12(5)	5975.6→4967.0		0.97(8)[j]		$14^- \rightarrow 12^-$

Table I cont.

E_γ^a (keV)	I_γ	$E_i \rightarrow E_f$ (keV)	R'	R''	A_2	$J_i^\pi \rightarrow J_f^\pi$
1009.4	40(9)	2503.5→1494.1	1.35(22)[e]	0.93(7)[e]		$6^+ \rightarrow 4^+$
1028.4	18(7)	4815.9→3787.5	1.42(19)[d]	1.04(11)[d]		$10^+ \rightarrow 8^+$
1050.4	23(9)	6263.9→5213.5	1.47(12)[c]	0.88(10)[c]		$15^- \rightarrow 13^-$
1076.7	8(3)	4120.9→3044.2	1.08(25)[e]	0.81(14)[e]	−0.21(21)	$9^+ \rightarrow 8^+$
1077.2	4(2)	11740+x→10664+x			+0.12(23)	$(24^+ \rightarrow 22^+)$
1134.8	≤1	2628.9→1494.1				$5^- \rightarrow 4^+$
1143.8	4(2)	12311+x→11168+x				$(25^+ \rightarrow 23^+)$
1145.3	10(4)	7120.9→5975.6		1.08(18)[j]		$16^- \rightarrow 14^-$
1150.6	24(9)	9250.4→8099.8	1.59(26)[d]	1.07(14)[d]		$20^+ \rightarrow 18^+$
1211.4	4(2)	12951+x→11740+x				$(26^+ \rightarrow 24^+)$
1253.6	15(6)	7517.5→6263.9	1.31(22)[f]	0.93(11)[f]	+0.68(32)	$17^- \rightarrow 15^-$

Table I cont.

E_γ^a (keV)	I_γ	$E_i \rightarrow E_f$ (keV)	R'	R''	A_2	$J_i^\pi \rightarrow J_f^\pi$
1284.5	17(7)	3787.5→2503.5				$8^+ \rightarrow 6^+$
1290.1	4(2)	8411.0→7120.9		0.91(20)[j]		$18^- \rightarrow 16^-$
1295.9	10(4)	3787.5→2491.8				$8^+ \rightarrow 6^+$
1302.6	4(2)	13614+x→12311+x				$(27^+ \rightarrow 25^+)$
1310.6	12(5)	10561.0→9250.4	1.45(27)[e]	1.05(14)[e]		$22^+ \rightarrow 20^+$
1366.5	9(4)	8884.0→7517.5		1.06(11)[f]		$19^- \rightarrow 17^-$
1382.3	3(1)	14322+x→12951+x				$(28^+ \rightarrow 26^+)$
1452.1	2(1)	15065+x→13614+x				$(29^+ \rightarrow 27^+)$
1465.8	6(2)	10349.8→8884.0		1.01(15)[f]		$21^- \rightarrow 19^-$
1466.0	3(2)	9877.0→8411.0		1.15(28)[j]		$20^- \rightarrow 18^-$
1471.5	7(3)	2104.7→632.8				$4^+ \rightarrow 2^+$

Table I cont.

E_γ^a (keV)	I_γ	$E_i \rightarrow E_f$ (keV)	R'	R''	A_2	$J_i^\pi \rightarrow J_f^\pi$
1487.6	6(3)	12048.6→10561.0		0.87(20)[e]		$24^+ \rightarrow 22^+$
1529.0	2(1)	15861+x→14322+x				$(30^+ \rightarrow 28^+)$
1591.4	<2	11941.4→10349.8				$23^- \rightarrow 21^-$
1622.6	5(2)	9722+x→8100+x				$(20^+ \rightarrow 18^+)$
1677.6	3(2)	13726.2→12048.6				$26^+ \rightarrow 24^+$
1857.4	≤1	15583.6→13726.2				$28^+ \rightarrow 26^+$

[a])Errors range from 0.2 keV to 1.5 keV.

[b])From 187 keV gate.

[c])From 645 keV gate.

[d])From 808 keV gate.

[e])From sum of 808,892,1150 and 1028 keV gates.

[f])From 645+1050 keV gate.

[g])From 1009 keV gate.

[h])From 861 keV gate.

[i])From 997 keV gate.

[j])From 598 keV gate.

TABLE II. Transitions observed above the 4660 keV isomer.

E_γ (keV)	I_γ[a]	$E_i \rightarrow E_f$ (keV)	E_γ (keV)	I_γ[a]	$E_i \rightarrow E_f$ (keV)
147.9[b]	3(1)		488.5[b]	5(1)	
219.1[b]	1(0.5)		517.9	12(2)	(5770→5253)
274.9[b]	1(0.5)		542.4	6(1)	(6100→5558)
304.9	6(1)	(5558→5253)	552.2[b]	3(1)	
319.9	5(1)	(5573→5253)	592.8	35(2)	5253→4660
330.5	7(1)	(6100→5770)	621.9	11(2)	(7480→6858)
392.1[b]	1(0.5)		659.7	11(2)	5913→5253
398.1[b]	1(0.5)		714.0[b]	2(1)	
414.2	4(1)	(5987→5573)	757.7	15(2)	(6858→6100)
468.5[b]	2(0.5)				

[a])Relative γ-ray intensity in 'earlies' spectrum.

[b])Not placed in level scheme.

TABLE III. Spherical and Nilsson orbitals close to the Fermi surface for $\beta_2 \sim 0.15$.

Particle	Configuration		CSM Notation	
	Spherical	Nilsson	$\alpha=-\frac{1}{2}$	$\alpha=+\frac{1}{2}$
Neutrons	$h_{\frac{11}{2}}$	$[550]\frac{1}{2}^-$	E	F
	$h_{\frac{11}{2}}$	$[541]\frac{3}{2}^-$	G	H
	$g_{\frac{7}{2}}$	$[411]\frac{3}{2}^+$	A	B
	$d_{\frac{5}{2}}$	$[413]\frac{5}{2}^+$	D	C
Protons	$g_{\frac{9}{2}}$	$[404]\frac{9}{2}^+$	c	d
	$g_{\frac{9}{2}}$	$[413]\frac{7}{2}^+$	a	b

TABLE IV. Parameters used for Dönau analysis of band 4.

K	Q_0 (eb)	RAL config.	$i_x^{(2)}$ ($\hbar$)	$g^{(2)}$	DAL config.	$i_x^{(1)}$ ($\hbar$)	$g^{(1)}$
9	2.0	$\nu(h_{\frac{11}{2}})^2$	10	-0.21^a	$\pi([404]^{\frac{9}{2}^+} \otimes [413]^{\frac{7}{2}^+})$	2	$+1.27^a$
13	2.0	$\nu(h_{\frac{11}{2}})^2$	10	-0.21^a	$\pi([404]^{\frac{9}{2}^+} \otimes [413]^{\frac{7}{2}^+}) \otimes \nu([411]^{\frac{3}{2}^+} \otimes [413]^{\frac{5}{2}^+})$	2	$+0.74^b$
5	2.0	$\nu(h_{\frac{11}{2}})^2$	10	-0.21^a	$\nu([411]^{\frac{3}{2}^+} \otimes [413]^{\frac{5}{2}^+})$	2	-0.13^a
5	2.4	$\nu(h_{\frac{11}{2}})^2$	10	-0.21^a	$\pi([413]^{\frac{7}{2}^+} \otimes [431]^{\frac{1}{2}^+})$	4	$+1.20^a$

[a])From reference [24].

[b])From references [22,23].

TABLE V. Branching ratios and deduced $|g_K - g_R|$ values in band 4.

I_i	E_1 (keV)	E_2 (keV)	$\frac{I_\gamma(\Delta I=1)}{I_\gamma(\Delta I=2)}$	$\frac{B(M1)}{B(E2)}$ $(\frac{\mu_N^2}{eb^2})$	$\lvert g_K - g_R \rvert^a$
(21)	439	842	3.5(2.0)	12(7)	0.89(21)
(22)	503	942	1.0(0.6)	4(2)	0.51(17)
(23)	504	1007	1.3(0.8)	7(4)	0.69(20)
(24)	573	1077	1.0(0.7)	5(3)	0.60(20)
(25)	571	1144	1.0(0.7)	7(5)	0.70(22)
(26)	640	1211	1.0(0.7)	7(5)	0.68(22)
(27)	663	1303	1.0(0.7)	9(5)	0.78(23)
(28)	719	1382	0.7(0.4)	7(4)	0.67(24)
(29)	733	1452	1.0(0.7)	11(7)	0.88(26)
(30)	796	1529	1.0(0.7)	11(7)	0.89(26)

[a])Assumes K=5 and Q_0=2.4 eb.

Figure Captions

Figure 1: Experimental DCO ratios in ^{106}Cd for the ^{16}O+^{94}Zr (R') and ^{34}S+^{76}Ge (R") reactions. The full and dashed lines correspond to the expected values for pure, stretched quadrupole and dipole transitions respectively.

Figure 2: Partial decay scheme of ^{106}Cd constructed in the present work.

Figure 3: Partial decay scheme of ^{106}Cd, showing states fed by the 12^+ isomer.

Figure 4: (a) Spectrum of 'earlies' obtained from a sum of gates on the 224, 336, 552, 633, 646, 861, 875, 998, 1009 and 1069 keV transitions below the 12^+ isomer in ^{106}Cd. (b) Spectrum obtained from out-of-beam, prompt-$\gamma - \gamma$ gate on the 633 keV, $2^+_1 \rightarrow 0^+_1$ transition in ^{106}Cd.

Figure 5: Prompt $\gamma - \gamma$ spectrum for band 1 obtained from the sum of the 981, 1151, 1311 and 1488 keV gates from the ^{34}S+^{76}Ge reaction.

Figure 6: Gamma-gamma-time projections, from the ^{16}O+^{94}Zr data, between (a) the prompt 808 and 892 keV transitions (b) the 602 and 981 keV transitions and (c) transitions across the τ=33 ns $\frac{11}{2}^-$ isomer [21] in ^{103}Pd.

Figure 7: Prompt $\gamma - \gamma$ spectrum for band 2, gating on the 598 keV transition, for the ^{34}S+^{76}Ge reaction.

Figure 8: Prompt $\gamma - \gamma$ spectrum for band 3 from the sum of the 646, 890, 1050 and 1254 keV gates and the ^{34}S+^{76}Ge reaction.

Figure 9: Prompt $\gamma - \gamma$ spectra for band 4 from the sum of the 439 and 572 keV gates and the ^{34}S+^{76}Ge reaction.

Figure 10: Total Routhian surface calculations for the (0,+) configurations in ^{106}Cd at rotational frequencies of (a) 0.506 MeV/$\hbar$ ($I \approx 8\ \hbar$) (b) 0.569 ($I \approx 18\ \hbar$) (c) 0.632 MeV/$\hbar$ ($I \approx 22\ \hbar$) and (d) 0.695 MeV/$\hbar$ ($I \approx 24\ \hbar$).

Figure 11: CSM calculations for (a) neutrons and (b) protons in ^{106}Cd. The parameters used were β_2=0.16, β_4=-0.005, γ=0°, Δ_ν=1.08 MeV and Δ_π=1.20 MeV.

Figure 12: Experimental alignments in ^{106}Cd. Reference parameters of $\mathcal{I}_0$=7.0 $\hbar^2$/MeV and $\mathcal{I}_1$=15.0 $\hbar^4$/MeV^3 were used for all the bands.

Figure 13: Excitation energies of the 10^+ $\nu(h_{\frac{11}{2}})^2$ (top) and $\frac{11}{2}^-$ states (bottom) through the Cd isotopes.

Figure 14: Comparison of experimental and calculated B(M1)/B(E2) ratios for band 4. See table IV for details of the parameters used for the various calculated configurations.

REFERENCES

[1] J. Kampulainen, R. Julin, J. Kantele, A. Passoja, W.H. Trzaska, E. Verho, J. Käärämäki, D. Cuoiu and M. Ivascu, *Phys. Rev.* **C45** (1992) 640

[2] P.H. Regan, G.D. Dracoulis, G.J. Lane, P.M. Walker, S.S. Anderssen, A.P. Byrne, P.M. Davidson, T. Kibédi, A.E. Stuchbery and K.C. Yeung, *J. Phys.* **G19** (1993) L157

[3] D. Jerrestam, F. Lidén, J. Gizon, L. Hildingsson, W. Klamra, R. Wyss, D. Barnéoud, J. Kownacki, Th. Lindblad, and J. Nyberg, *Nucl. Phys.* **A545** (1992) 835

[4] P.H. Regan, J.S. Middleton, K.R. Pohl, J.E. Bush, P.E. Raines, D.P. Balamuth, S.M. Mullins, A. Galindo-Uribarri, V.P. Janzen, D. Ward and S. Pilotte *Phys. Rev.* **C49** (1994) 1885

[5] S. Juutinen, P. Šimeček, C. Fahlander, R. Julin, J. Kumpulainen, A. Lampinen, T. Lönnroth, A. Maj, S. Mitarai, D. Müller, J. Nyberg, M. Piiparinen, M. Sugawara, I. Thorslund, S. Törmänen and A. Virtanen, *in press, Nucl. Phys.* **A** (1994)

[6] I. Thorslund, C. Fahlander, J. Nyberg, S. Juutinen, R. Julin, M. Piiparinen, R. Wyss, A. Lampinen, T. Lönnroth, D. Müller, S. Törmänen and A. Virtanen, *Nucl. Phys.* **A564** (1994) 285

[7] I. Thorslund, C. Fahlander, J. Nyberg, M. Piiparinen, R. Julin, S. Juutinen, A. Virtanen, D. Müller, H. Jensen and M. Sugawara, *Nucl. Phys.* **A568** (1993) 306

[8] M. Piiparinen, R. Julin, S. Juutinen, A. Virtanen, P. Ahonen, C. Fahlander, J. Hattula, A. Lampinen, T. Lönnroth, A. Maj, S. Mitarai, D. Müller, J. Nyberg, A. Pakkanen, M. Sugawara, I. Thorslund and S. Törmänen, *Nucl. Phys.* **A565** (1993) 671

[9] S. Juutinen, R. Julin, P. Ahonen, C. Fahlander, J. Hattula, J. Kumpulainen, A. Lampinen, T. Lönnroth, D. Müller, J. Nyberg, A. Pakkanen, M. Piiparinen, I. Thorslund, S. Törmänen and A. Virtanen, *Z. Phys.* **A336** (1990) 475

[10] S. Juutinen, R. Julin, M. Piiparinen, P. Ahonen, B. Cederwall, C. Fahlander, A. Lampinen, T. Lönnroth, A. Maj, S. Mitarai, D. Müller, J. Nyberg, P. Šimeček, M. Sugawara, I. Thorslund, S. Törmänen, A. Virtanen and R. Wyss, *Nucl. Phys.* **A573** (1994) 306

[11] Dan Jerrestam, B. Cederwall, B. Fogelberg, A. Gizon, J. Gizon, L. Hildingsson, E. Ideguchi, W. Klamra, J. Kownacki, F. Lidén, Th. Lindblad, S. Mitarai and J. Nyberg, *Nucl. Phys.* **A571** (1994) 393

[12] G.D. Dracoulis and A.P. Byrne, *Annual Report 1989* **ANU-P/1052** 115

[13] H. R. Andrews *Proposal for a National Facility, The 8π Spectrometer,* AECL/8329 (1984)

[14] A. Galindo-Uribarri, *Prog. Part. Nucl. Phys.* **28** (1992) 463

[15] A.P. Byrne, K. Schiffer, G.D. Dracoulis, B. Fabricius, T. Kibédi, A.E. Stuchbery and K.P. Lieb, *Nucl. Phys.* **A548** (1992) 131

[16] G.J. Lane, G.D. Dracoulis, A.P. Byrne, P.M. Walker, A.M. Baxter, J.A. Sheikh and W. Nazarewicz *in press, Nucl. Phys.* **A** (1994)

[17] L.E. Samuelson, J.A. Grau, S.I. Popik, F.A. Rickey and P.C. Simms, *Phys. Rev.* **C19** (1979) 73

[18] J. Daniére, R. Béraud, R. Rougny, J. Genevy-Rivier, and J. Tréherne, *Z. Phys.* **A280** (1977) 363

[19] W. Andrejtscheff, L.K. Kostov, H. Rotter, H. Prade and F. Stary, M. Senba, N. Toupas, Z.Z. Ding and P. Raghavan, *Nucl. Phys.* **A437** (1985) 167

[20] W. Klamra and E. Dafni, *Z. Phys.* **A334** (1989) 515

[21] W. Dietrich, B. Nyman, A. Johansson and A. Bäcklin, *Physica Scripta* **12** (1975) 80

[22] P.Raghavan, *Atomic and Nuclear Data Tables* **42** (1989) 189

[23] D.A. Volkov, B.I. Gorbachev, A.I. Kovalenko, A.I. Levon, O.F. Nemets and O.V. Sevastyuk, *Yad. Fiz.* **44** (1986) 849 and *Sov. Jour. Nucl. Phys.* **44** (1986) 547

[24] T. Lönnroth, S. Vajda, O.C. Kistner and M.H. Rafailovich, *Z. Phys.* **A317** (1984) 317

[25] W. Nazarewicz, R. Wyss and A. Johnson, *Nucl. Phys.* **A503** (1989) 285

[26] R. Wyss, J. Nyberg, A. Johnson, R. Bengtsson and W. Nazarewicz, *Phys. Lett.* **B215** (1988) 211

[27] R. Bengtsson, S. Frauendorf and F.R. May, *At. Nucl. Data. Tab.* **35** (1986) 15

[28] F. Dönau, *Nucl. Phys.* **A471** (1987) 469

[29] J.A. Grau, L.E. Samuelson, F.A. Rickey, P.C. Simms and G.J. Smith, *Phys. Rev.* **C14** (1976) 2297

[30] A.O. Macchiavelli, J. Burde, R.M. Diamond, C.W. Beausang, M.A. Deleplanque, R.J. McDonald, F.S. Stephens and J.E. Draper, *Phys. Rev.* **C38** (1988) 1088

[31] K.R. Pohl, P.H. Regan, J.E. Bush, P.E. Raines, D.P. Balamuth, A. Galindo-Uribarri, D. Ward, V.P. Janzen, S.M. Mullins and S. Pilotte, *Bull. Am. Phys. Soc.* **38** (1993) 1857

[32] L.K. Kostov, W. Andrejtscheff, H. Rotter, H. Prade and F. Stary *Phys. Lett.* **123B** (1983) 29

[33] J.H. Degraaf *et al.*, Proc. of the Conference on Physics from Large Gamma-ray Detector Arrays, Berkeley, CA Aug. 2-6 July, 1994 (LBL-35687) Vol. 1 p.49.

[34] Dan Jerrestam, S. Mitarai, E. Ideguchi, B. Fogelberg, A. Gim, J. Gizon, W. Klamara, Th. Lindblad, R. Bark, J. Nyberg, M. Piiparinen and G. Sletten, *Nucl. Phys.* **A557** (1993) 411c

[35] R. Wadsworth, H.R. Andrews, R.M. Clark, D.B. Fossan, A. Gallindo-Uribarri, J.R. Hughes, V.P. Janzen, D.R. LaFosse, S.M. Mullins, E.S. Paul, D.C. Radford, H. Schnare, P. Vaska, D. Ward, J.N. Wilson and R. Wyss, *Nucl. Phys.* **A559** (1993) 461

[36] D.C. Radford, Proceedings of the International Seminar on the Frontier of Nuclear Spectroscopy, ed. Y. Yoshizawa, H. Kusakari and T. Otsuka, World Scientific, 1993, p. 229

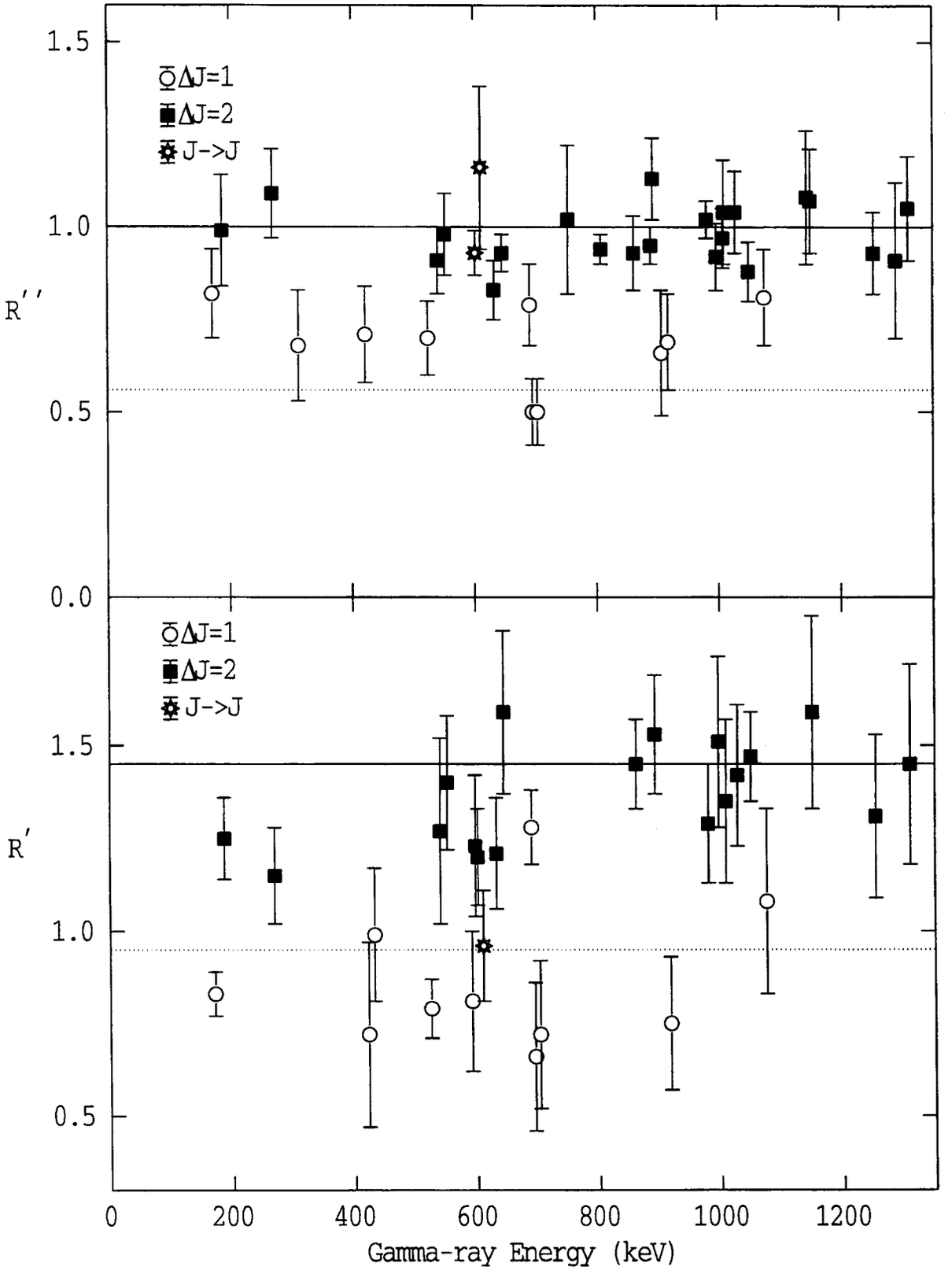
ΔJ=1
ΔJ=2
J->J
R''
R'
Gamma-ray Energy (keV)

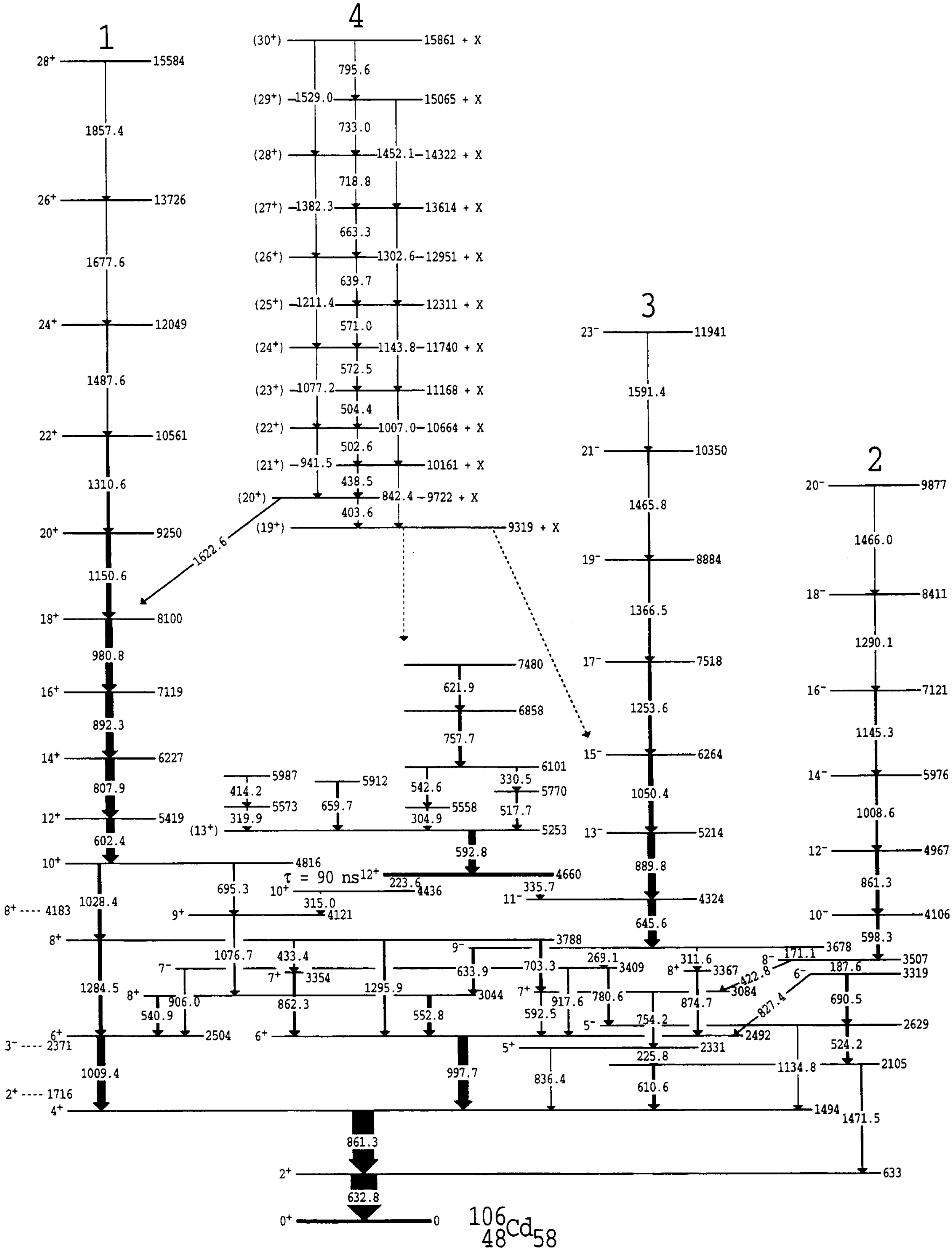

1
2
3
4
(30+) 15861 + X
(29+) 15065 + X
(28+) 14322 + X
(27+) 13614 + X
(26+) 12951 + X
(25+) 12311 + X
(24+) 11740 + X
(23+) 11168 + X
(22+) 10664 + X
(21+) 10161 + X
(20+) 9722 + X
(19+) 9319 + X
795.6
1529.0
733.0
1452.1
718.8
1382.3
663.3
1302.6
639.7
1211.4
571.0
1143.8
572.5
1077.2
504.4
1007.0
502.6
941.5
438.5
842.4
403.6
1622.6
28+ 15584
1857.4
26+ 13726
1677.6
24+ 12049
1487.6
22+ 10561
1310.6
20+ 9250
1150.6
18+ 8100
980.8
16+ 7119
892.3
14+ 6227
807.9
12+ 5419
602.4
10+ 4816
1028.4
8+ ---- 4183
8+
1284.5
6+
3- ---- 2371
1009.4
2+ ---- 1716
4+
23- 11941
1591.4
21- 10350
1465.8
19- 8884
1366.5
17- 7518
1253.6
15- 6264
1050.4
13- 5214
889.8
11- 4324
645.6
20- 9877
1466.0
18- 8411
1290.1
16- 7121
1145.3
14- 5976
1008.6
12- 4967
861.3
10- 4106
598.3
7480
621.9
6858
757.7
6101
5987
414.2
5573
319.9
5912
659.7
542.6
5558
304.9
330.5
5770
517.7
(13+) 5253
592.8
τ = 90 ns 12+ 4660
223.6
10+ 4436
335.7
315.0
9+ 4121
695.3
1076.7
433.4
7+ 3354
7-
906.0
8+
540.9
2504
862.3
1295.9
633.9
3044
552.8
6+
997.7
9-
703.3
3788
269.1
3409
7+
917.6
592.5
780.6
5-
754.2
8+
311.6
3367
874.7
422.8
3084
8-
171.1
3678
3507
6-
187.6
3319
827.4
2492
690.5
2629
524.2
2105
5+
2331
225.8
836.4
610.6
1134.8
1494
1471.5
861.3
2+
633
632.8
0+
0
106 48 Cd 58

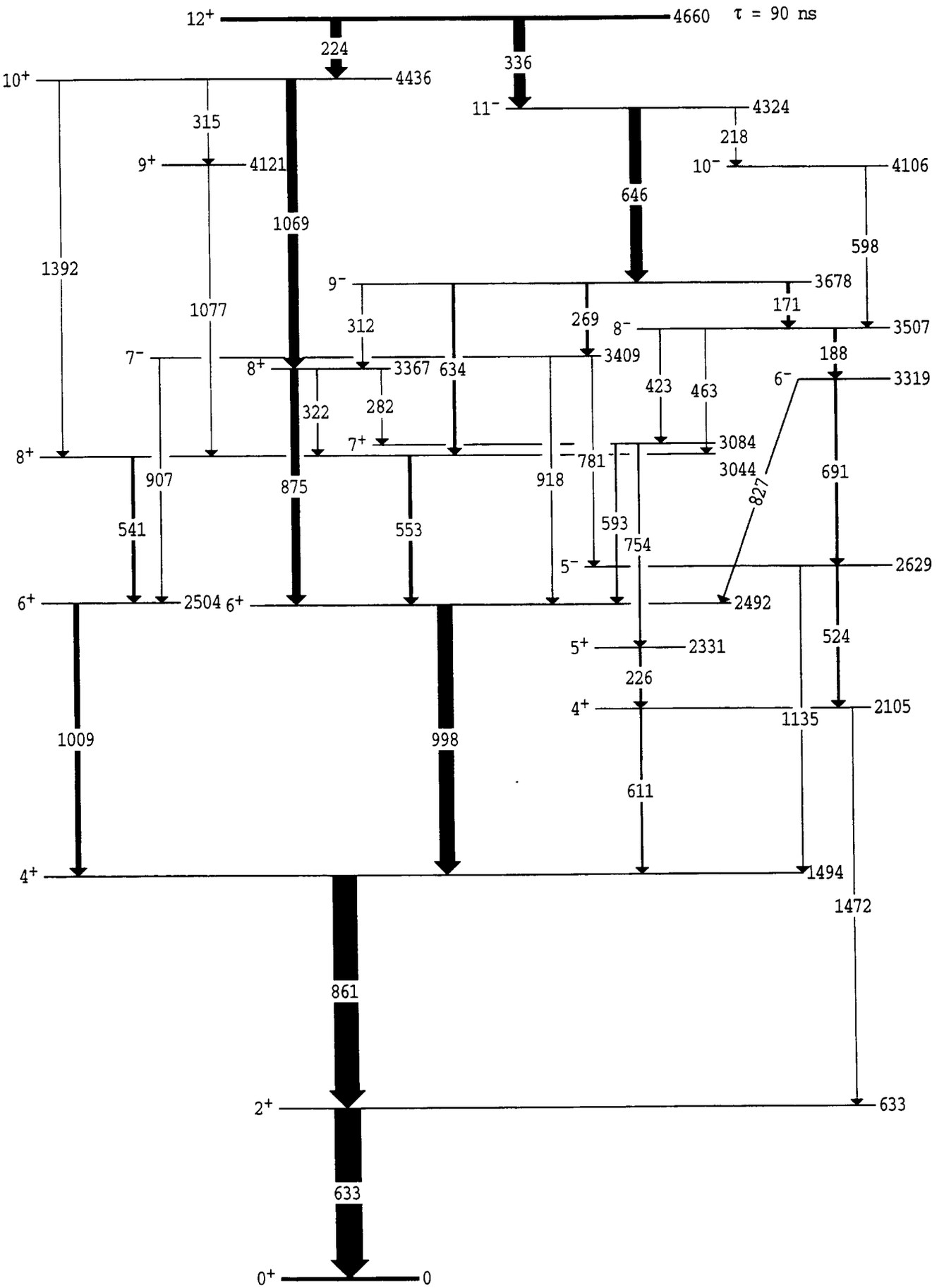
12+
4660
τ = 90 ns
224
336
10+
4436
11−
4324
315
218
9+
4121
10−
4106
646
1069
598
1392
9−
3678
171
1077
312
269
8−
3507
7−
8+
3367
634
3409
188
6−
3319
423
463
322
282
7+
3084
8+
781
3044
691
907
875
918
827
541
553
593
754
5−
2629
6+
2504
6+
2492
524
5+
2331
226
4+
2105
1135
1009
998
611
4+
1494
1472
861
2+
633
633
0+
0

$^{106}_{48}Cd_{58}$

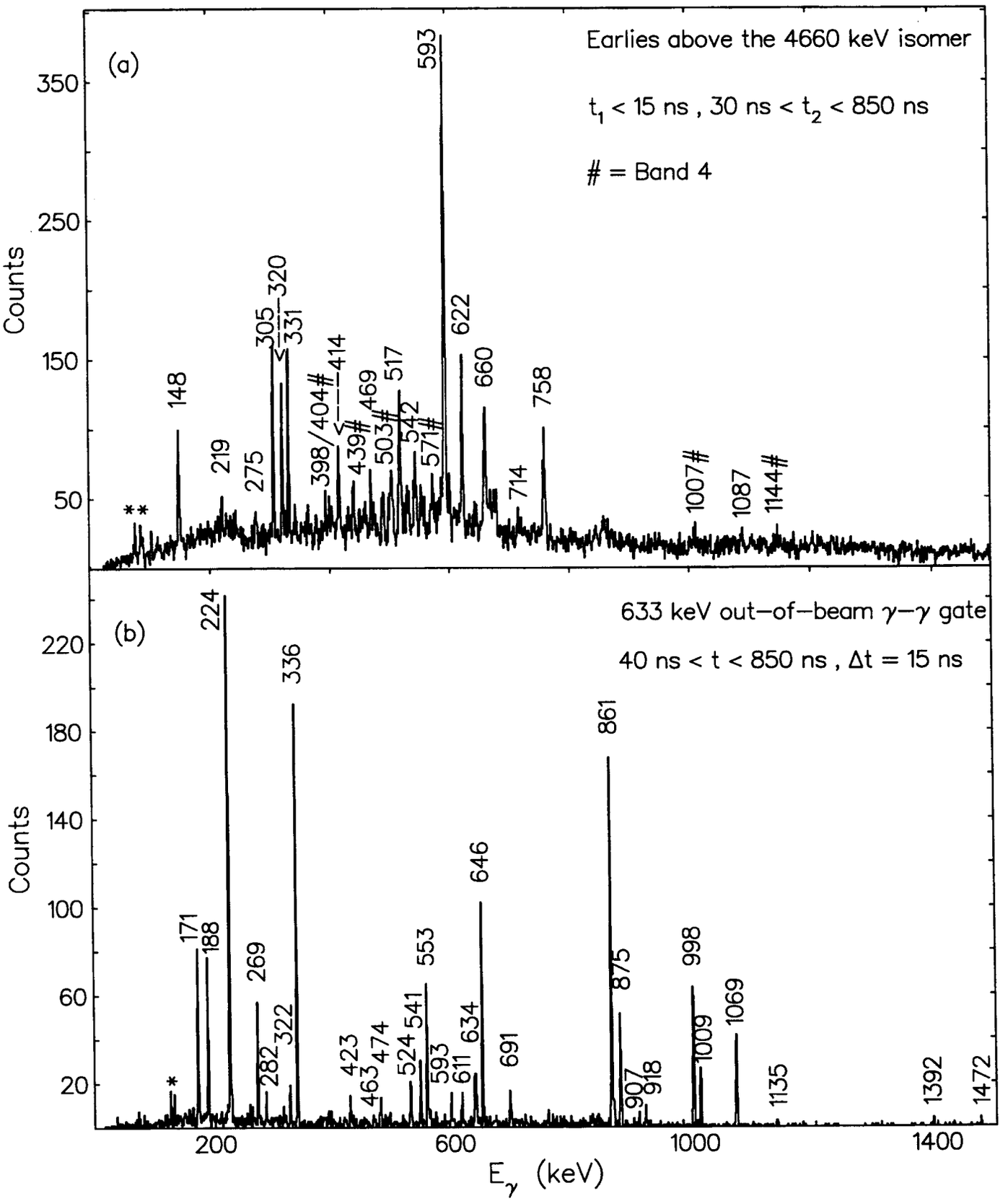
(a)
Earlies above the 4660 keV isomer
t_1 < 15 ns , 30 ns < t_2 < 850 ns
= Band 4
Counts
350
250
150
50
593
622
660
758
305
320
331
414
148
219
275
398/404#
439#
469
503#
517
542
571#
714
1007#
1087
1144#
**
(b)
633 keV out–of–beam γ–γ gate
40 ns < t < 850 ns , Δt = 15 ns
Counts
220
180
140
100
60
20
224
336
861
646
171
188
269
322
553
541
524
423
463
474
593
611
634
691
875
998
1069
1009
907
918
1135
1392
1472
*
200
600
1000
1400
E_γ (keV)

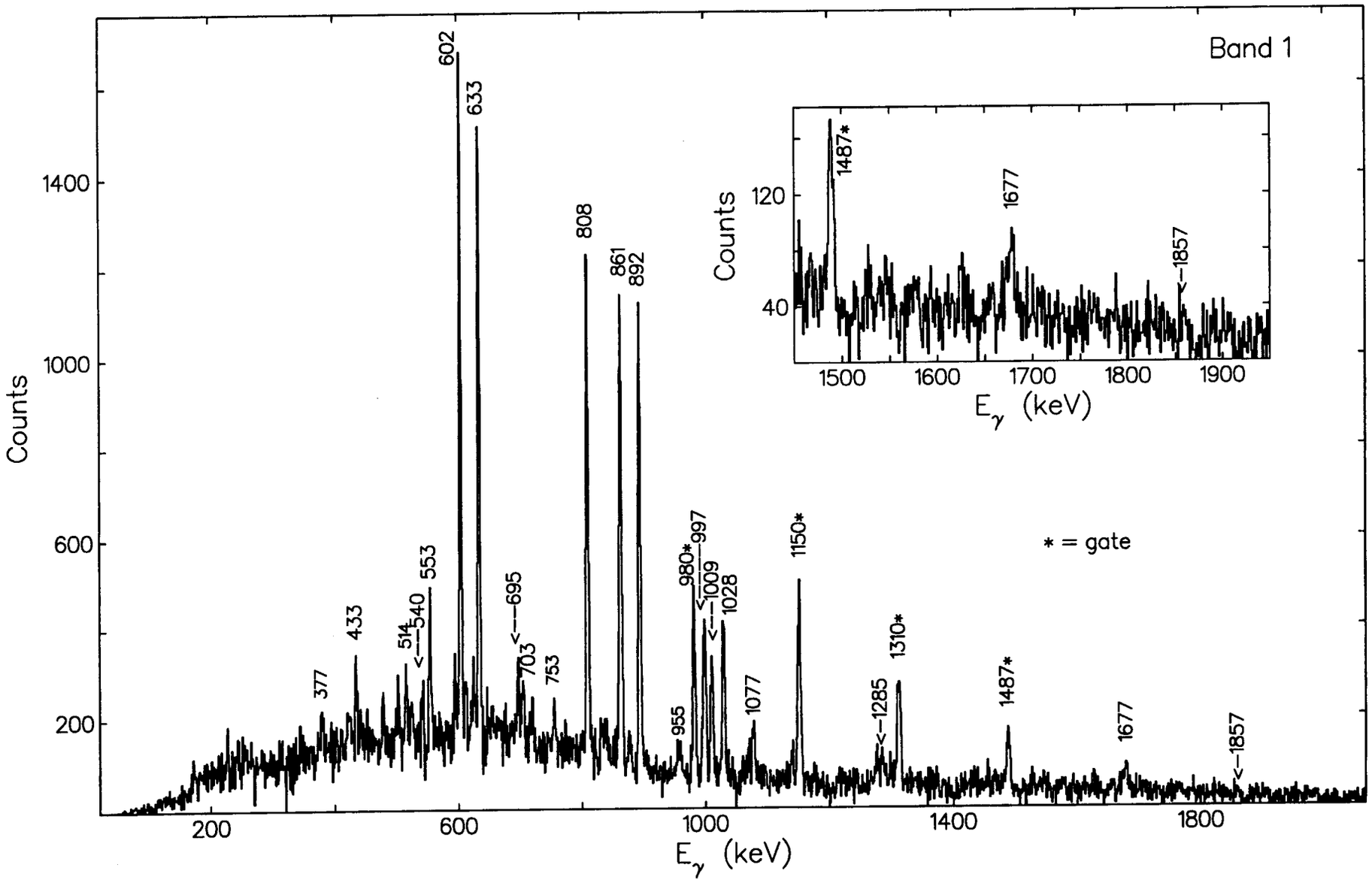
Band 1
Counts
E_γ (keV)
602
633
808
861
892
433
514
540
553
695
703
753
955
980*
997
1009
1028
1077
1150*
1285
1310*
1487*
1677
1857
* = gate
Counts
E_γ (keV)
1487*
1677
1857

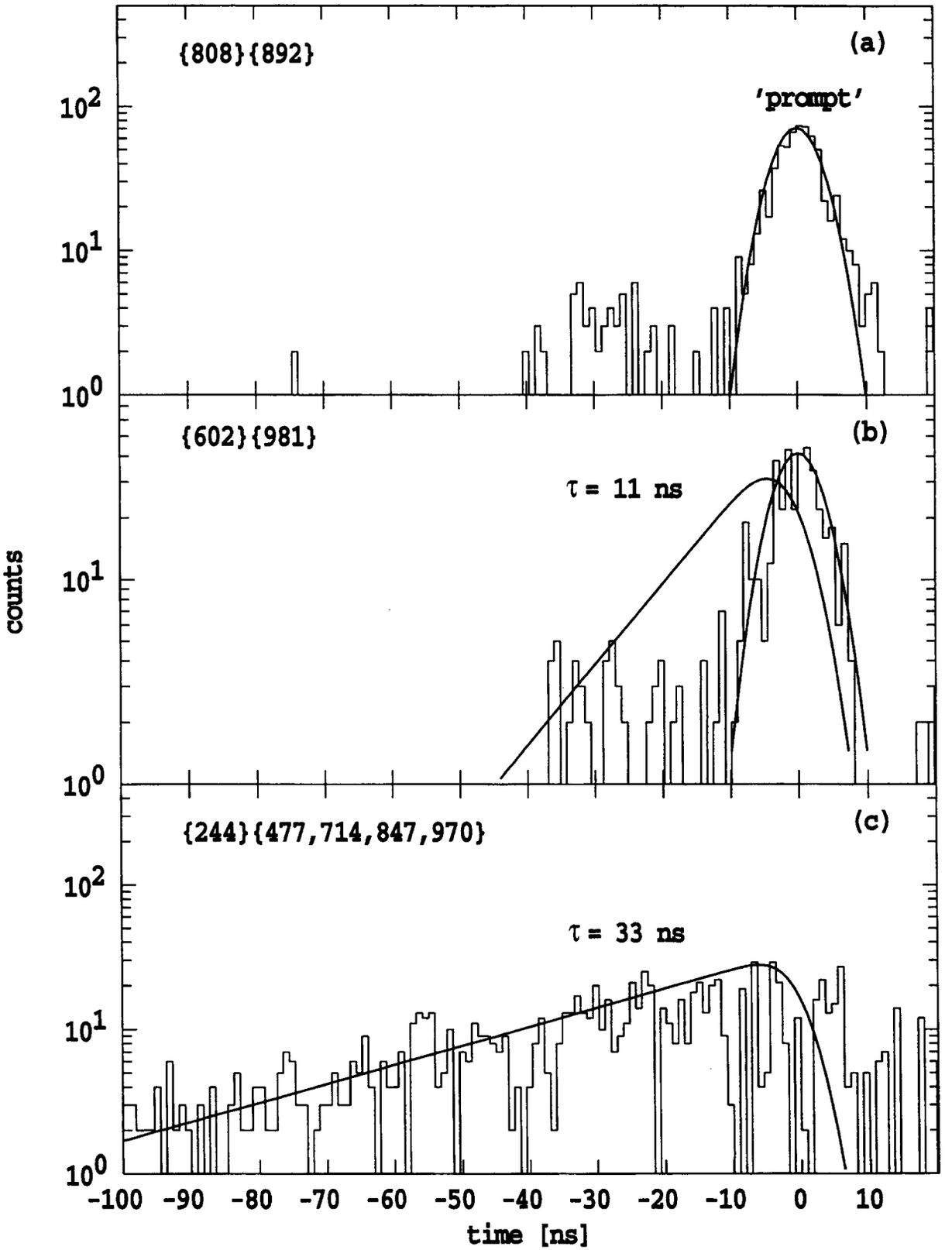
{808}{892}
(a)
'prompt'
{602}{981}
(b)
τ = 11 ns
{244}{477,714,847,970}
(c)
τ = 33 ns
counts
time [ns]

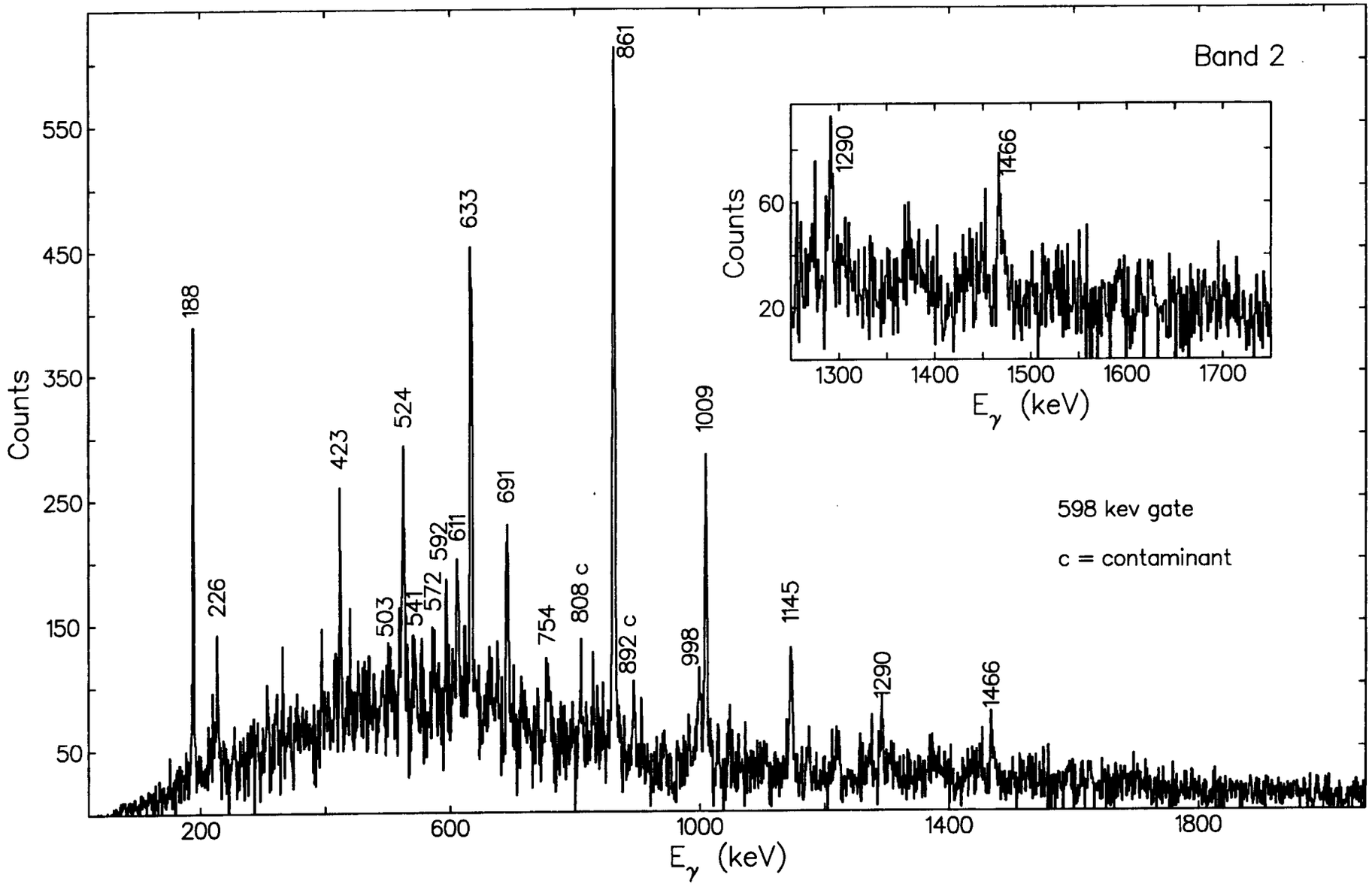
Band 2
Counts
550
450
350
250
150
50
188
226
423
503
524
541
572
592
611
633
691
754
808 c
861
892 c
998
1009
1145
1290
1466
200
600
1000
1400
1800
E_γ (keV)
598 kev gate
c = contaminant
Counts
60
20
1290
1466
1300
1400
1500
1600
1700
E_γ (keV)

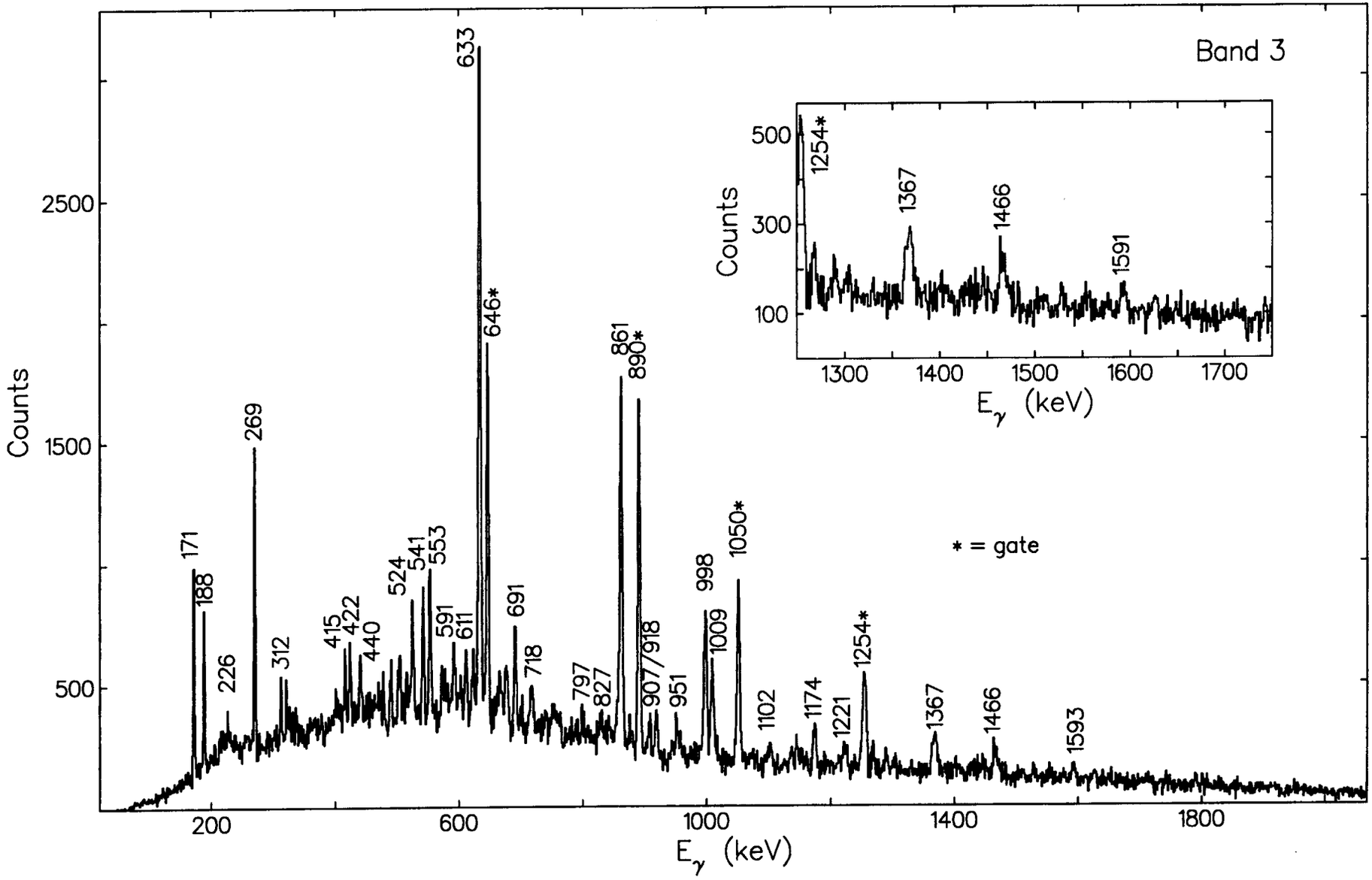
Band 3
Counts
2500
1500
500
200
600
1000
1400
1800
E_γ (keV)
633
646*
269
861
890*
171
188
226
312
415
422
440
524
541
553
591
611
691
718
797
827
907/918
951
998
1009
1050*
1102
1174
1221
1254*
1367
1466
1593
* = gate
Counts
500
300
100
1300
1400
1500
1600
1700
E_γ (keV)
1254*
1367
1466
1591

Band 4
* = gate
Counts
E_γ (keV)
171
188
226
269
<---305
<---320
332
404
433
439*
475
503
524
541
553
572*
593
<---598
<---602
611
633
640
646
663
691
703
719
733
<--- 796
808
827
842
861
874
890/892
926
942
981
998
1009
1028
1050
1077
1136
1144
1211
1254
1303
1382
1452
1472
1529
1623

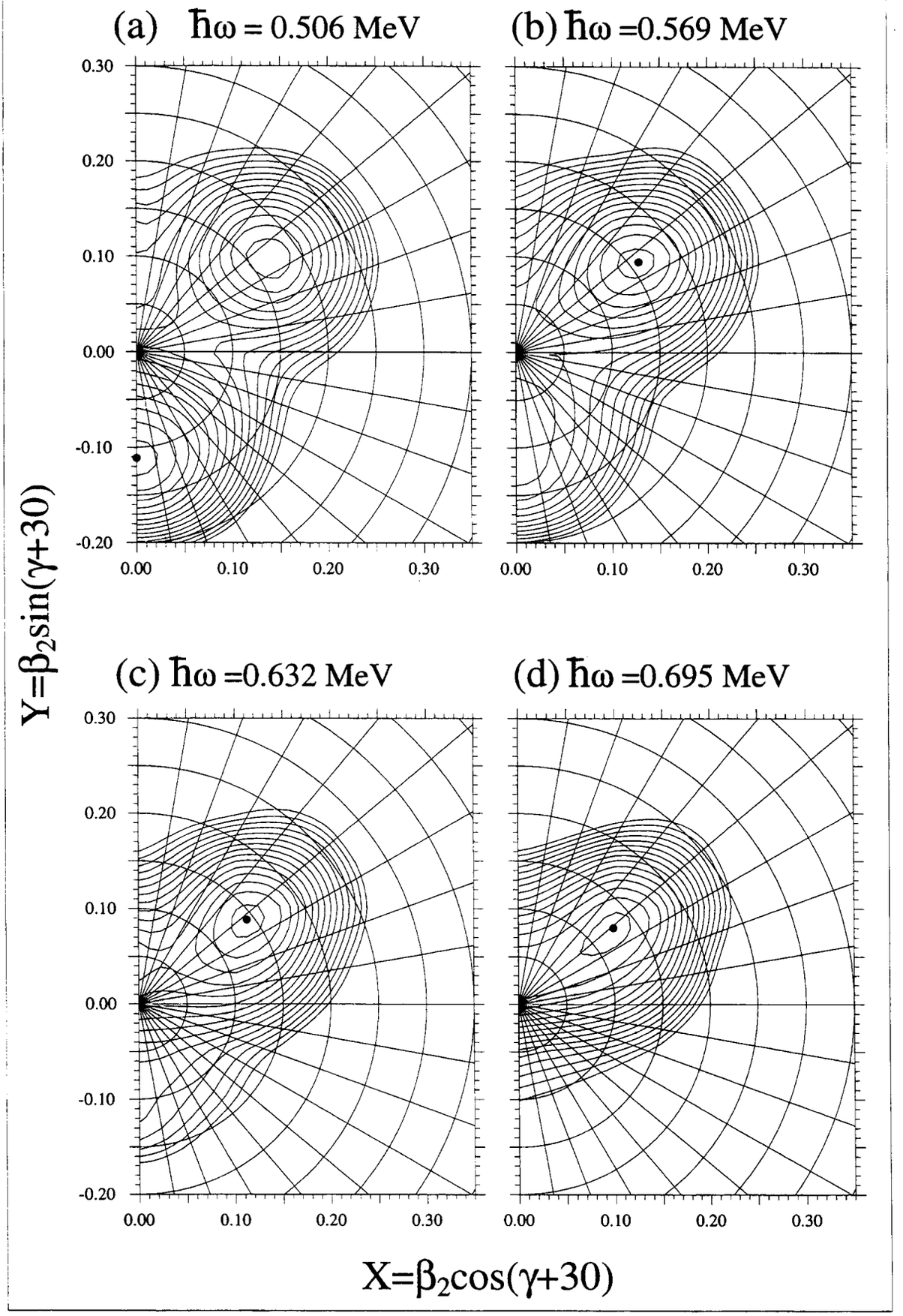
(a) ħω = 0.506 MeV
(b) ħω =0.569 MeV
(c) ħω =0.632 MeV
(d) ħω =0.695 MeV
0.30
0.20
0.10
0.00
-0.10
-0.20
0.00
0.10
0.20
0.30
Y=β2sin(γ+30)
X=β2cos(γ+30)

(a)

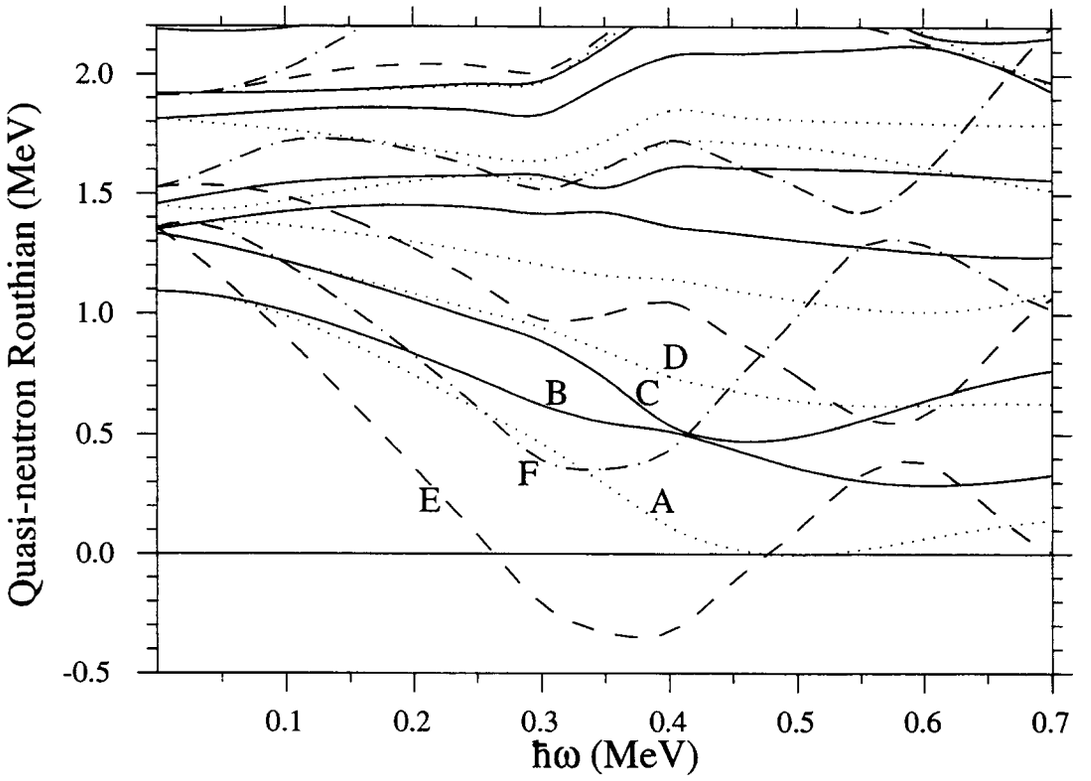
Quasi-neutron Routhian (MeV)
2.0
1.5
1.0
0.5
0.0
-0.5
0.1
0.2
0.3
0.4
0.5
0.6
0.7
ħω (MeV)
A
B
C
D
E
F

(b)

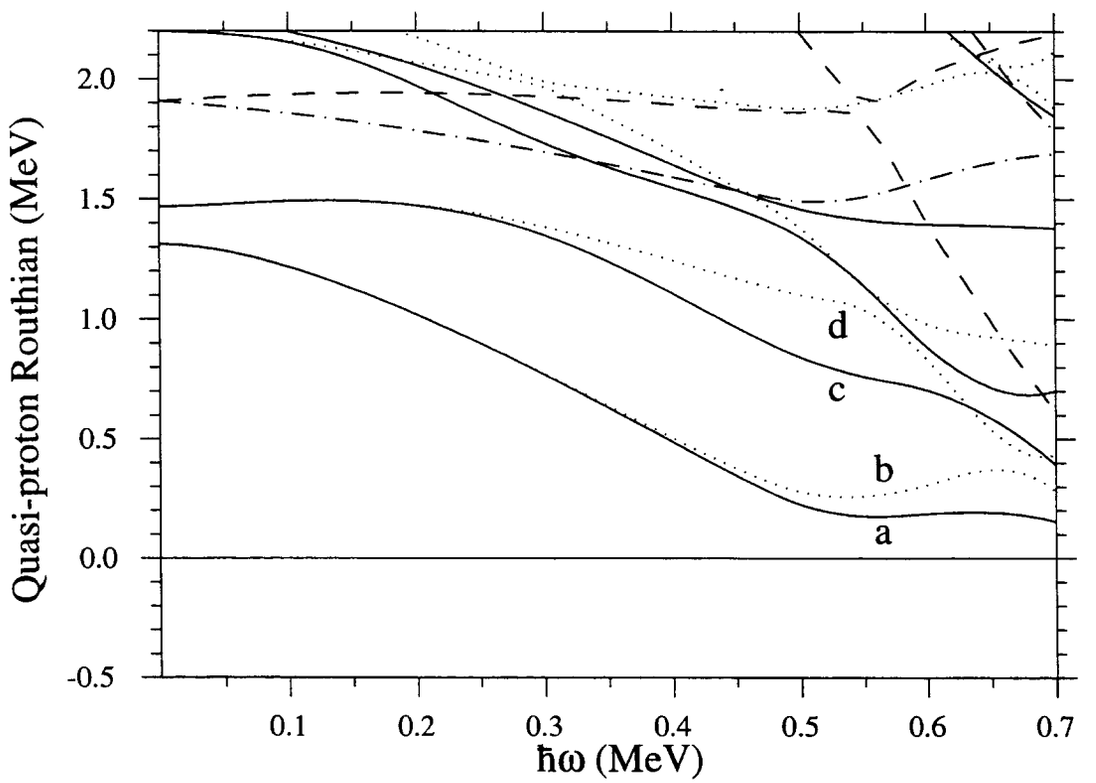
Quasi-proton Routhian (MeV)
2.0
1.5
1.0
0.5
0.0
-0.5
0.1
0.2
0.3
0.4
0.5
0.6
0.7
ħω (MeV)
a
b
c
d

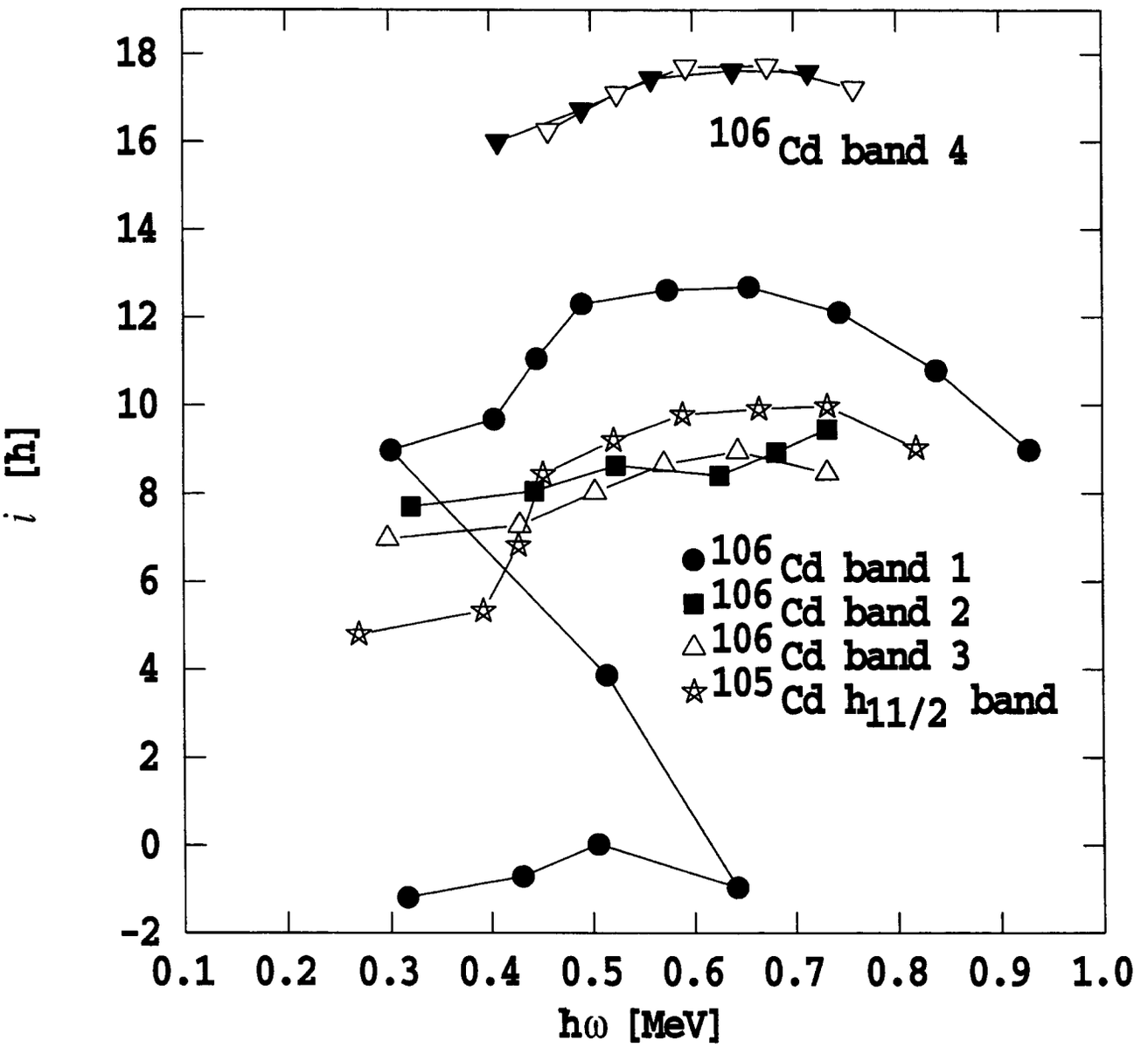
18
16
14
12
10
8
6
4
2
0
-2
0.1
0.2
0.3
0.4
0.5
0.6
0.7
0.8
0.9
1.0
i [h]
hω [MeV]
106 Cd band 4
106 Cd band 1
106 Cd band 2
106 Cd band 3
105 Cd h11/2 band

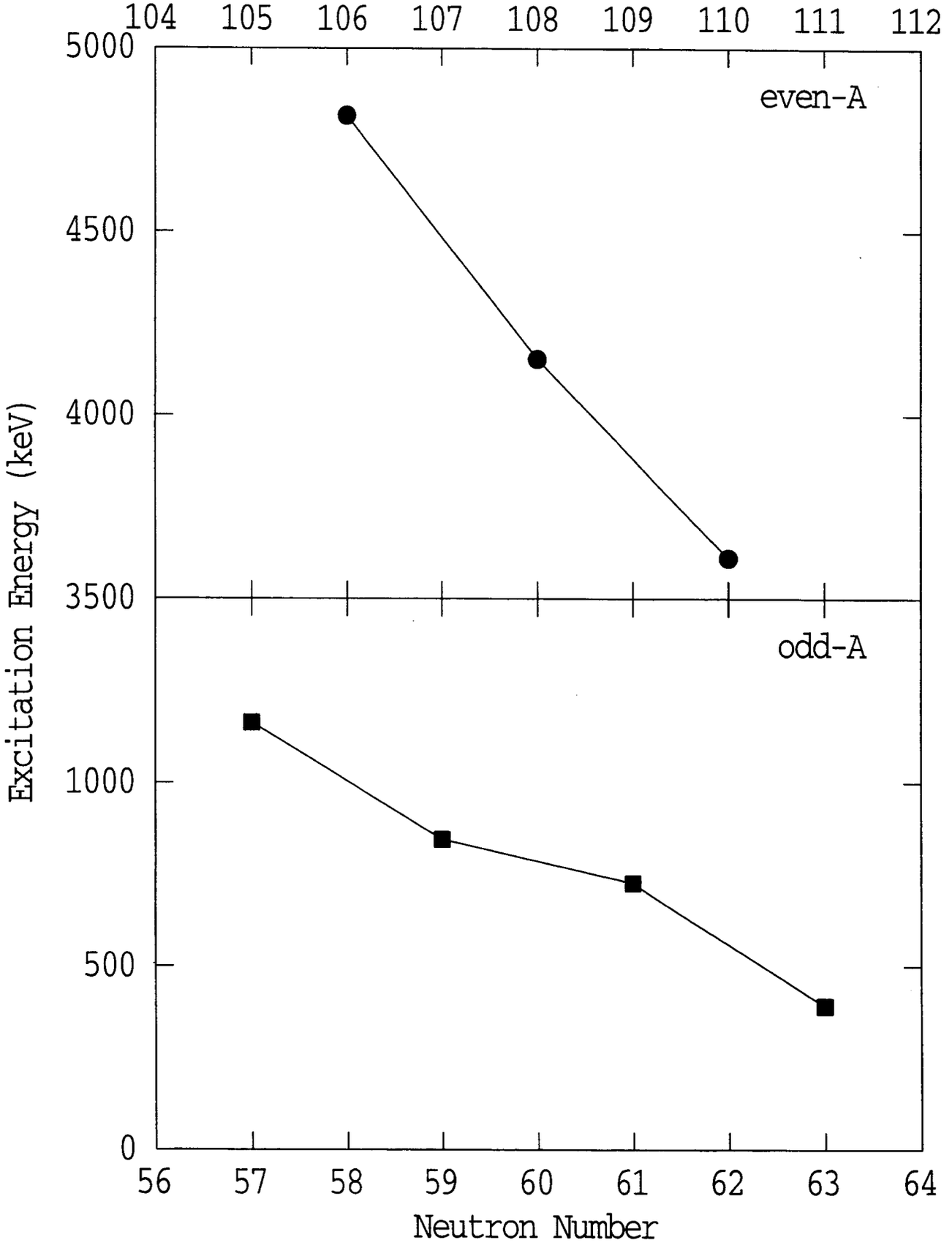
104
105
106
107
108
109
110
111
112
5000
4500
4000
3500
1000
500
0
even-A
odd-A
Excitation Energy (keV)
56
57
58
59
60
61
62
63
64
Neutron Number

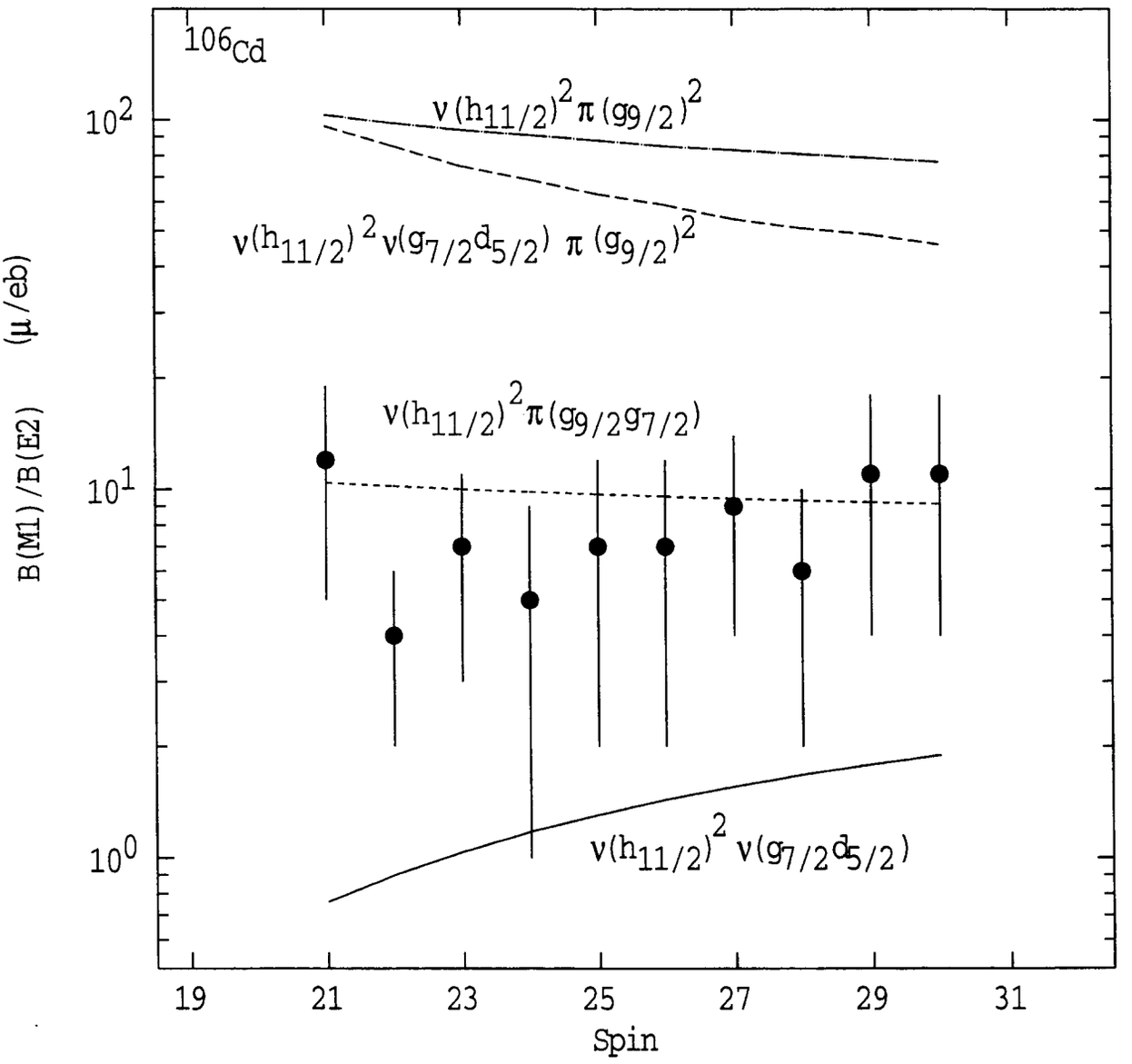
106Cd
ν(h11/2)2π(g9/2)2
ν(h11/2)2ν(g7/2d5/2) π (g9/2)2
ν(h11/2)2π(g9/2g7/2)
ν(h11/2)2 ν(g7/2d5/2)
B(M1)/B(E2) (μ/eb)2
10^2
10^1
10^0
19
21
23
25
27
29
31
Spin